Article
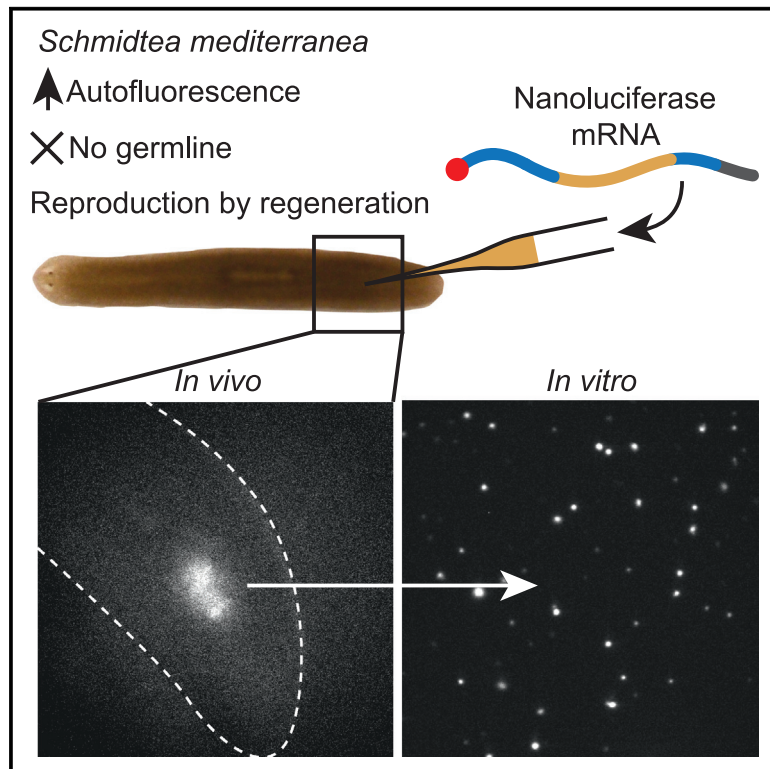
Heterologous reporter expression in the planarian *Schmidtea mediterranea* through somatic mRNA transfection

Graphical abstract

Highlights

- Planarian cells can be transfected *in vitro* and *in vivo*

- Nanoluciferase allows for sensitive transgene detection in autofluorescent tissue

- Luminescence imaging reveals expression kinetics in single cells and live animals

- UTR hacking identifies sequences in mRNA that modulate protein expression

Authors

Richard Nelson Hall, Uri Weill, Leonard Drees, ..., Andrew Z. Fire, Jochen C. Rink, Bo Wang

Correspondence

jochen.rink@mpinat.mpg.de (J.C.R.), wangbo@stanford.edu (B.W.)

In brief

Hall et al. demonstrate luminescence reporter expression from transfected mRNA in the regenerative planarian flatworm *Schmidtea mediterranea.* This study paves the way for developing additional transgenic techniques in planarians and provides a means to investigate post-transcriptional regulation of gene expression in this previously genetically intractable organism.

CellPress

Cell Reports Methods

Article

Heterologous reporter expression in the planarian *Schmidtea mediterranea* through somatic mRNA transfection

Richard Nelson Hall,[1,12] Uri Weill,[2,12] Leonard Drees,[2] Sergio Leal-Ortiz,[3] Hongquan Li,[4] Margarita Khariton,[1] Chew Chai,[1] Yuan Xue,[1] Benyamin Rosental,[5] Stephen R. Quake,[1,6,7] Alejandro Sánchez Alvarado,[8,9] Nicholas A. Melosh,[3] Andrew Z. Fire,[10,11] Jochen C. Rink,[2,*] and Bo Wang[1,13,*]

[1]Department of Bioengineering, Stanford University, Stanford, CA 94305, USA
[2]Department of Tissue Dynamics and Regeneration, Max Planck Institute for Multidisciplinary Sciences, Göttingen 37077, Germany
[3]Department of Materials Science and Engineering, Stanford University, Stanford, CA 94305, USA
[4]Department of Electrical Engineering, Stanford University, Stanford, CA 94305, USA
[5]The Shraga Segal Department of Microbiology, Immunology, and Genetics, Faculty of Health Sciences, Center for Regenerative Medicine and Stem Cells, Ben Gurion University of the Negev, Beer-Sheva 84105, Israel
[6]Department of Applied Physics, Stanford University, Stanford, CA 94305, USA
[7]Chan Zuckerberg Biohub, San Francisco, CA 94158, USA
[8]Stowers Institute for Medical Research, Kansas City, MO 64110, USA
[9]Howard Hughes Medical Institute, Kansas City, MO 64110, USA
[10]Department of Pathology, Stanford University School of Medicine, Stanford, CA 94305, USA
[11]Department of Genetics, Stanford University School of Medicine, Stanford, CA 94305, USA
[12]These authors contributed equally
[13]Lead contact
*Correspondence: jochen.rink@mpinat.mpg.de (J.C.R.), wangbo@stanford.edu (B.W.)
https://doi.org/10.1016/j.crmeth.2022.100298

MOTIVATION The study of planarians has contributed to advances in our understanding of regeneration, stem cell dynamics, and many other fundamental biological processes. However, the persistent challenge of expressing transgenes in planarians has led to the speculation that they may be resistant to transfection. Here, we develop methods to express exogenous mRNAs in both isolated planarian cells and whole animals by optimizing delivery techniques, genetic constructs, and detection methods. These methods allow us to study transfection kinetics and post-transcriptional regulation of gene expression in a quantitative manner. Beyond planarian research, this work should also provide a broadly applicable strategy to develop similar tools for other animals that are challenging to modify genetically.

SUMMARY

Planarians have long been studied for their regenerative abilities. Moving forward, tools for ectopic expression of non-native proteins will be of substantial value. Using a luminescent reporter to overcome the strong auto-fluorescence of planarian tissues, we demonstrate heterologous protein expression in planarian cells and live animals. Our approach is based on the introduction of mRNA through several nanotechnological and chemical transfection methods. We improve reporter expression by altering untranslated region (UTR) sequences and codon bias, facilitating the measurement of expression kinetics in both isolated cells and whole planarians using luminescence imaging. We also examine protein expression as a function of variations in the UTRs of delivered mRNA, demonstrating a framework to investigate gene regulation at the post-transcriptional level. Together, these advances expand the toolbox for the mechanistic analysis of planarian biology and establish a foundation for the development and expansion of transgenic techniques in this unique model system.

INTRODUCTION

Planarian flatworms have fascinated scientists with their regenerative abilities and have played a critical role in studies of

stem cells and regeneration (Newmark and Sánchez Alvarado, 2002; Reddien, 2018; Rink, 2018). Planarians can regenerate their entire body from a small tissue fragment. During this process, they restore their body axes and rebuild all organs with

appropriate proportions. While gene knockdown by RNA-mediated genetic interference (RNAi) (Sánchez Alvarado and Newmark, 1999; Reddien et al., 2005; Collins et al., 2010) and next-generation sequencing (Böser et al., 2013; Lakshmanan et al., 2016; Guo et al., 2017, 2022; Grohme et al., 2018; Fincher et al., 2018; Plass et al., 2018) have been widely used in planarian research, tools for transgene expression are lacking. Earlier efforts have attempted whole-animal electroporation of plasmid DNA encoding a fluorescence protein (González-Estévez et al., 2003), but the intense autofluorescence of planarian tissues and lack of orthogonal verification of transgene expression have limited the applicability of this study.

Establishing reporter expression in a system needs to overcome three challenges: construct delivery, expression, and detection. Delivery and expression are prerequisites for detection, while delivery and expression require reliable detection to optimize. In addition, strategies to circumvent genetic defense mechanisms (Kim et al., 2019; Chen et al., 2003; Aljohani et al., 2020) that may restrict transgene expression are difficult to test without a robust reporter. Therefore, the first demonstration of reporter expression is often the bottleneck for developing transgenic tools; establishing a positive control can transform the method development process from a random walk in a vast parameter space into a well-constrained optimization problem.

Injecting constructs into embryos often provides the first route for transgene expression in most systems. However, it is infeasible to inject in the ectolethical eggs of planarians, as blastomeres are tiny and dispersed among yolk cells (Cardona et al., 2006; Davies et al., 2017). Furthermore, the commonly used planarian strains of *Schmidtea mediterranea* are exclusively asexual, reproducing through fission and regeneration (Benazzi et al., 1972; Vila-Farré and Rink, 2018). This leaves the introduction of genetic material into somatic cells as the most general approach to genetic modification. While possible in some vertebrate models and immortalized cell lines, transformation protocols and reagents are typically optimized for specific systems. In addition, measuring delivery efficiency relies on expression as the ultimate readout. Due to the distant relationship between planarians and other model organisms, it is unclear what modifications to reporter constructs are needed to drive expression in planarians. Finally, autofluorescence limits the utility of fluorescent proteins in planarians, especially during the initial stages of reporter optimization, when signals may be weak.

Here, we report a robust and extensively verified method for heterologous gene expression in planarians. To address the problem of delivery, we used a direct nanoscale injection method to first establish a positive control, on which basis we identified efficacious chemical transfection reagents for transforming planarian cells both *in vitro* and *in vivo*. To circumvent the numerous variables associated with DNA transfections, we delivered synthetic mRNA to drive expression. Finally, for detection, we relied on luminescent reporters—in particular, a compact, bright, and stable luciferase, nanoluciferase (Nluc) (Hall et al., 2012; England et al., 2016). Using this sensitive and quantitative luminescence readout, we improved the reporter construct by altering untranslated regions and codon usage biases and presented a case study in which we identified regulatory sequences

that modulate gene expression post-transcriptionally. Via luminescence imaging, we quantified single-cell transfection kinetics and explored limiting factors in transgene expression in planarian cells. Finally, we demonstrated the utility of luminescence imaging for monitoring gene expression in live animals. Our results not only provide the first positive control for exogenous gene expression in planarians to guide the future development of planarian transgenesis, but also offer a new route to measure and understand gene expression and regulation in planarian cells.

RESULTS

Nluc mRNA delivered through nanostraws is expressed in planarian cells

To establish mRNA expression in the asexual strain of *S. mediterranea*, we sought to identify an efficient platform for delivering genetic material into primary planarian cells. We selected nanostraws, which combine the robustness of microinjection with the throughput of bulk electroporation (Tay and Melosh, 2019).

Nanostraws are 100- to 200-nm wide hollow aluminum oxide tubes protruding from a polycarbonate substrate above a buffer reservoir containing the genetic material to be delivered (Figures 1A and 1B). Cells are centrifuged against the straws to establish close contact. Electric pulses are then used to locally porate the membranes and electrophorese genetic material through the nanostraws and into the cellular cytoplasm (Figures S1A–S1C). By only permeabilizing membranes in contact with nanostraws, this approach improves both delivery efficiency and cell viability (Xie et al., 2013; Cao et al., 2018).

To prepare cells for nanostraw transfection, we flow-sorted a stem cell (i.e., neoblast)-enriched population based on their light-scattering properties, so-called X1FS, from dissociated planarians (Hayashi et al., 2006; Wagner et al., 2011). This population is uniform in size and depleted of debris, which improve nanostraw delivery. Our initial experiments used capped and polyadenylated *in vitro* transcribed mRNA encoding mScarlet fused to the planarian histone H2B. We reasoned that red fluorescence may be more easily detectable against planarian autofluorescence (Lim et al., 2019), which is biased toward shorter wavelengths, and that a nuclear localization signal may further enhance signal-to-noise. We used a pulse train protocol optimized for delivery in human hematopoietic stem cells, which have similar morphological characteristics with XIFS cells (i.e., small size, minimally adherent, high nucleus-to-cytoplasm ratio) (Schmiderer et al., 2020).

We performed flow cytometry to quantify fluorescence signal and found a broad distribution of fluorescence intensities spanning three orders of magnitude in both experimental and negative conditions (Figure S1D), making the assessment of transfection outcomes difficult. Since some cells genuinely exhibit brighter fluorescence than others, false positives may be common and true positives could be obscured by the broad autofluorescent background. These results compelled us to seek an alternative non-fluorescent reporter.

Unlike fluorophores, luciferases produce light through oxidative chemical reactions of a substrate (luciferin), and most animal tissues are devoid of autoluminescence (Figure 1C). Therefore, we delivered mRNA encoding a planarian codon optimized Nluc
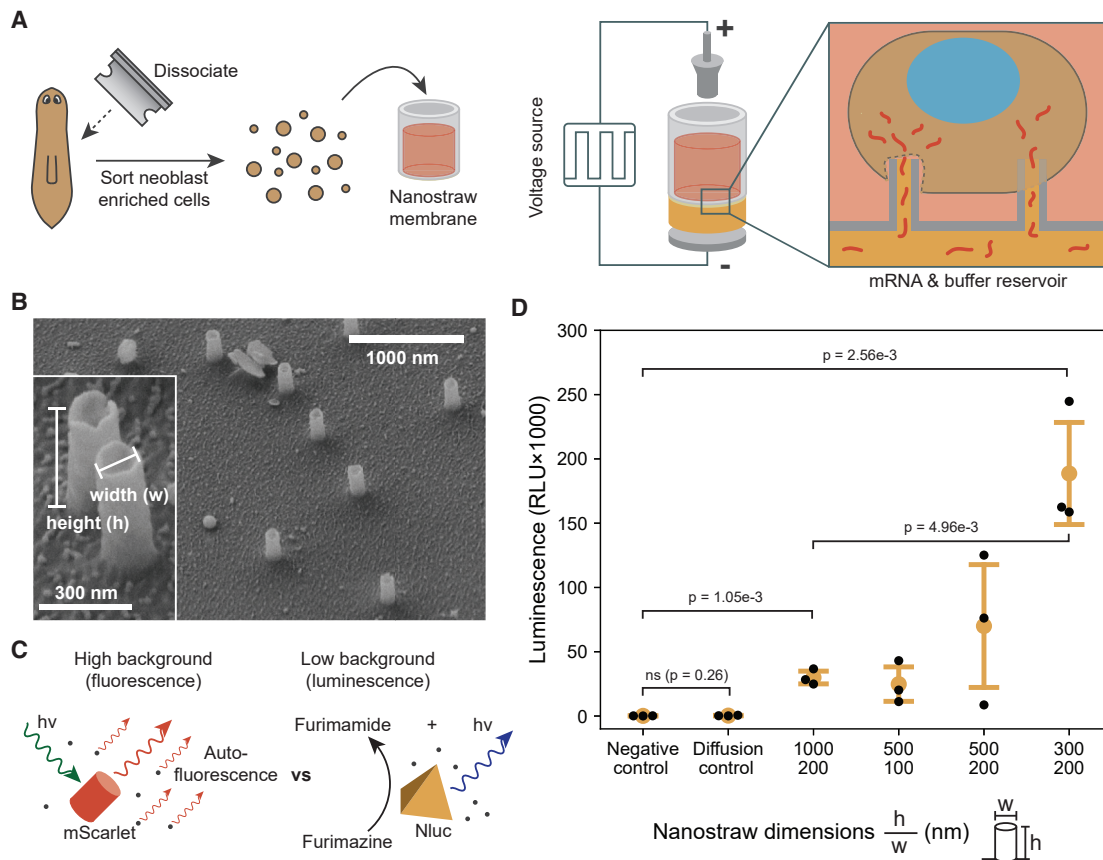
Figure 1. Nluc mRNA delivered through nanostraws is expressed in planarian cells

(A) Schematics showing the steps of nanostraw delivery. In each experiment, 200,000 cells are placed into a nanostraw cartridge and electroporated with square wave pulses between 2 titanium electrodes.

(B) SEM images of nanostraws. Inset: a magnified view of individual straws.

(C) Unlike autofluorescence, autoluminescence is absent in planarian tissues, making luminescent reporters easy to detect.

(D) Luminescence from 200,000 cells at 24 hour post transfection (hpt) with sNluc1 mRNA. Negative control: Nanostraw delivery with PBS alone. Diffusion: Mock experiments without applying electrical pulses. Luminescence is measured with NanoGlo-Live substrate by plate reader. Each data point represents one biological replicate conducted on an independently isolated population of cells using nanostraws from the same batch and mRNA synthesized in the same reaction. Error bars: SDs. Statistical analysis is performed with 1-way ANOVA (p = 8.05e−5) in addition to 2-sided Welch's t test to calculate p values between pairs of conditions; ns: not significant (p > 0.05).

See also Figure S1.

(sNluc1) (see STAR Methods) into X1FS cells. Transfected cells were maintained for 24 h in Iso-L15, a nutrient rich medium with reduced osmolarity. A similar medium has been shown to improve planarian cell viability (Lei et al., 2019). We observed a clear and reproducible luminescence signal in transfected cells over 100-fold above the background of the negative controls. The physical dimensions of the nanostraws strongly influenced the signal, as previously observed (Xie et al., 2013), implying that expression was dependent on the amount of mRNA delivered (Figure 1D). Overall, these results provide a proof-of-principle for heterologous protein expression in planarian cells.

A screen identifies chemical reagents to efficiently transfect planarian cells

With a validated reporter construct, we next sought to identify a more accessible mRNA delivery method. Chemical transfection reagents have become increasingly popular because of their ease of use, high efficiency, and scalability, but they are often developed and optimized for specific cell types.

To identify reagents for planarian cell transfection, we screened commercially available reagents by transfecting sNluc1 mRNA containing 5′ and 3′ untranslated region (UTR) sequences from a highly expressed planarian gene, Y-box binding protein (*YB1*, dd_Smed_v6_52_0_1). Our screen used total cells from freshly dissociated animals rather than X1FS cells due to the large number of transfections needed (Figure 2A). While most transfection reagents produced little to no expression using the manufacturer's recommended protocols (see STAR Methods), Viromer and Mirus *Trans*IT reagents, both of which comprise endoosmolytic cationic polymers, achieved luminescent signals 100- to 1,000-fold above the negative control (Figure 2B).

To further optimize the transfection protocols, we tested various ratios between Nluc mRNA and reagent components (Figures 2C and 2D). For Viromer, increasing the amount of reagent and/or mRNA doubled the signal, with 0.8 μL reagent per 1 μg mRNA per reaction as an economic compromise for further experiments. A similar 2-fold boost was achieved for *Trans*IT, but maximal signal intensities remained below those of Viromer transfections. These conditions, however, produced luminescence ~100-fold lower compared to transfections of mammalian cells (e.g., HeLa cells) (Figures S2A and S2B), indicating that future optimizations may achieve substantially higher expression levels.

To confirm that luminescence was produced by transfected cells, we imaged cells using NanoGlo-Live furimazine (Fz) substrate (Promega) on an LV200 bioluminescence imaging system (Olympus). Individual luminescent cells were evident in transfected samples (Figure S3), but never observed in negative controls. High magnification confirmed the cytoplasmic origin of the luminescence signal. By counting luminescent live cells over time, we quantified the transfection efficiency to be ~3.5% out of all of the cells for Viromer, which plateaued at ~12 h post-transfection (hpt), and 0.2% for *Trans*IT (Figure 2E), whereas cell viability was similar after both transfections (Figure 2F). Comparing the reagents, the discrepancy in the percentage of luminescent cells is smaller than the difference in total luminescence intensity measured by plate reader, suggesting that Viromer transfected more cells and produced higher expression per cell. Finally, to further demonstrate that Nluc mRNA is the source of the luminescence, we created a Nluc variant with a premature stop codon, which abolished expression (Figure S2C). Overall, these observations establish chemical delivery as a viable method for mRNA transfection of planarian cells, with Viromer and *Trans*IT as promising leads.

Altering UTR sequences and codon bias improves Nluc expression

With efficient delivery reagents, we sought to improve the reporter construct. To identify UTRs that may enhance expression, we flanked sNluc1 with UTRs (Figures S4 and S5A–S5C) from four endogenous genes with high expression in all cell types. These UTRs either increased (*RPL15* [ribosomal protein L15, dd_Smed_v6_193_0_1], *YB1*, *RPL10* [ribosomal protein L10, dd_Smed_v6_130_0_1]) or decreased (*ENO*, enolase, dd_Smed_v6_510_0_1) the expression of Nluc relative to the construct lacking endogenous UTRs (Figure 3A).

Next, we investigated the effect of codon optimization, the commonplace practice of matching endogenous codon biases to maximize expression (Quax et al., 2015; Jeacock et al., 2018). This may be important for *S. mediterranea*, in which a strong preference for A/T at third-base positions contributes to a genome-wide A/T bias of 70% (Grohme et al., 2018). We generated five codon-optimized Nluc variants, besides sNluc1, to cover a range of codon adaptation indices (CAIs), a 0–1 bounded value measuring the codon bias of the gene compared to a reference codon table (Sharp and Li, 1987; Puigbò et al., 2008). We also included a Nluc sequence optimized for mammalian expression (hNluc) as a comparison. Unexpectedly, the luminescence in transfected cells did not correlate with CAI

(Figure 3B). The most highly expressed construct (sNluc2, CAI = 0.713) was part of a series of constructs with similar CAIs and GC contents generated by randomly sampling the planarian codon table (sNluc2–4, see STAR Methods). Based on these results, we combined RPL15 UTRs and sNluc2 into an improved reporter construct that was used for all subsequent experiments unless otherwise specified (Figure S5D).

Live luminescence imaging reveals expression kinetics *in vitro*

Quantifying expression levels across and within single cells can help reveal kinetics of transfection and gene expression. For quantitative microscopy, we built a customized luminescence microscope (Kim et al., 2017). Using a demagnifying tube lens, we expanded the field-of-view (FOV) of high magnification/high numerical aperture (NA) objectives needed for efficient light collection. In addition, we used a back-illuminated electron multiplying charge-coupled device (EMCCD) camera (Andor iXon) for detection, which has single-photon sensitivity and provides quantitative measurements. The conventional substrate for Nluc, Fz, has poor water solubility and is supplied in organic solvents, which may stress cells and affect gene expression kinetics. To overcome this, we used a Fz derivative, fluorofurimazine (FFz), which has improved water solubility and thereby reduces cytotoxicity while maintaining the brightness of Nluc (Su et al., 2020).

With these advances, we quantified the distribution of luminescence intensities across transfected cells. For this experiment, bulk dissociated cells were allowed to adhere to a glass-bottom imaging well treated with concanavalin A to prevent them from moving in and out of the imaging plane. We imaged cells at 24 hpt, as at this time point, the number of luminescent cells should have plateaued (Figure 2E). In a single FOV (~1.6 mm^2), we captured over 80 individual luminescing cells (Figure 4A). From these images, we segmented cells and quantified their luminescence at 40 min post-FFz addition, ensuring that FFz diffused into the cells. This revealed a long-tailed distribution with a small number of intensely bright cells (Figure 4B). Unexpectedly, we captured new transfection events at this late time point, indicating that not only were these cells healthy enough to be transfected but also that there remained functional Viromer-mRNA complexes in the media (Figure 4C).

Motivated by the observation that we could capture individual transfection events, we performed imaging from the moment of transfection to measure the transfection kinetics and the onset of expression. After adding transfection complexes and FFz simultaneously, the sample started dark, but within the first hour, cells began to luminesce (Figure 4D; Video S1). We quantified the luminescence of each cell (Figure 4E) and extracted the transfection time, defined by when the signal exceeds the background noise. The transfection time followed a gamma distribution with a mean of ~140 min post-transfection (mpt) (Figure 4F), suggesting that transfections are independent stochastic events, although the rate of transfection likely varies over time. This timescale is consistent with the fast kinetics of mRNA transfection and translation (Leonhardt et al., 2014). Most cells reached their maximal luminescence rapidly, whereas a few cells grew luminescent over a longer period (Figure 4G). To quantify
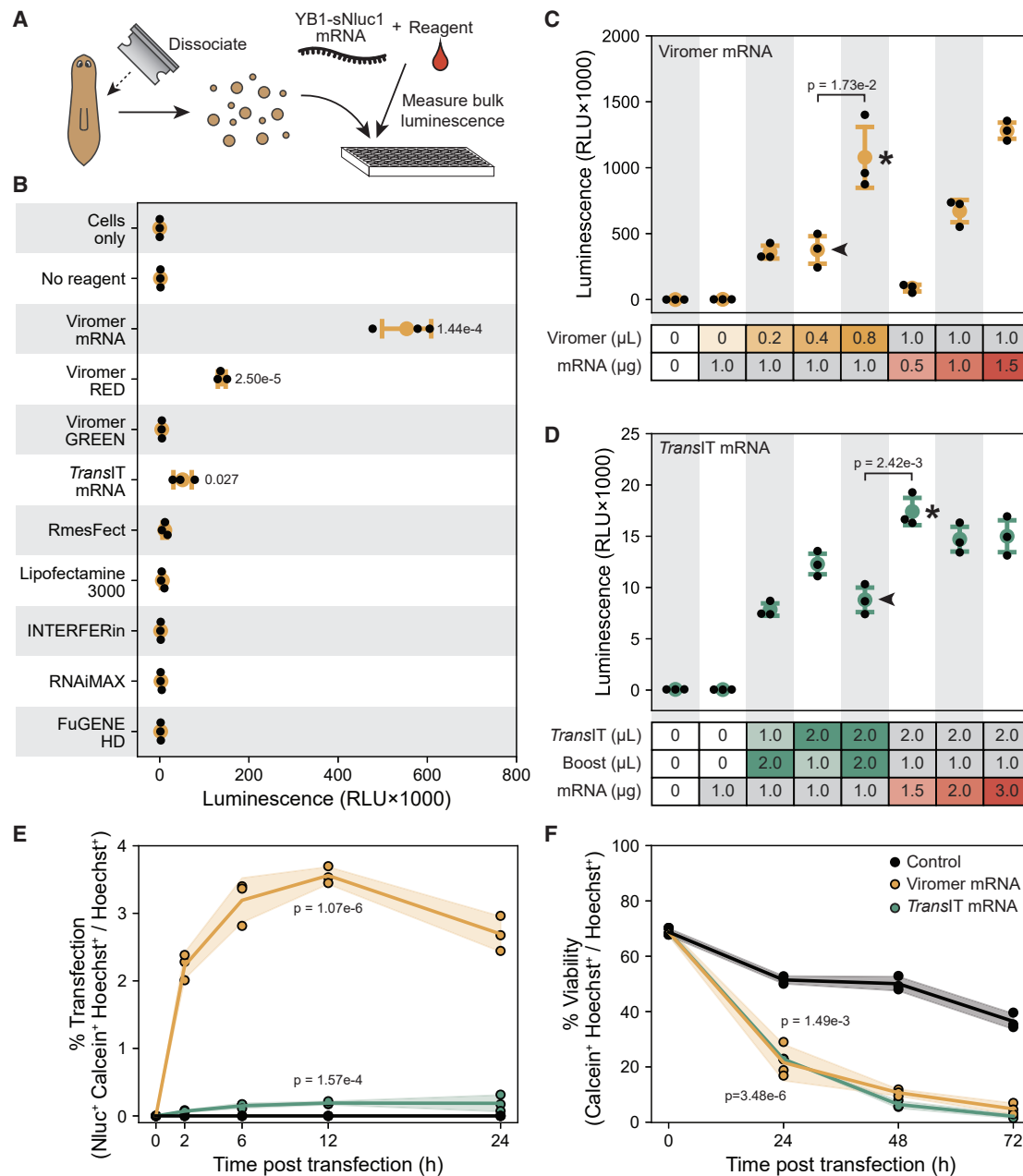
Figure 2. A screen identifies chemical reagents to efficiently transfect planarian cells

(A) A diagram of the chemical transfection reagent screen.

(B) Luminescence from 200,000 cells transfected with 1 μg YB1-sNluc1 mRNA delivered by chemical transfection reagents, using the manufacturer's recommended protocols, assayed at 24 hpt.

(C and D) Optimization of Viromer mRNA (C) and *Trans*IT mRNA (D) identifies conditions with increased expression that are used for all following experiments (asterisk), compared to the condition initially used in the screen (arrowheads).

(E) Percentage of luminescent cells (Nluc$^+$Calcein$^+$Hoechst$^+$/Hoechst$^+$) over the course of 24 hpt.

(F) Cellular viability (Calcein$^+$Hoechst$^+$/Hoechst$^+$) over the course of 72 hpt. Control cells are left untransfected.

Statistics: Data points in (B) represent the mean of technical replicates (n = 3) for each biological replicate. Data points in (C)–(F) represent technical replicates using mRNA prepared from the same batch. Error bars: SDs. ANOVA: p = 2.08e−18 (B); p = 1.25e−9 (C); p = 2.05e−11 (D). p values for pairwise comparison are calculated using 2-sided Welch's t test and reported in the figure. In (B), (E), and (F), comparisons are made by comparing experimental groups with the negative control in which mRNA is delivered with no transfection reagent.

See also Figures S2, S3, and S9.
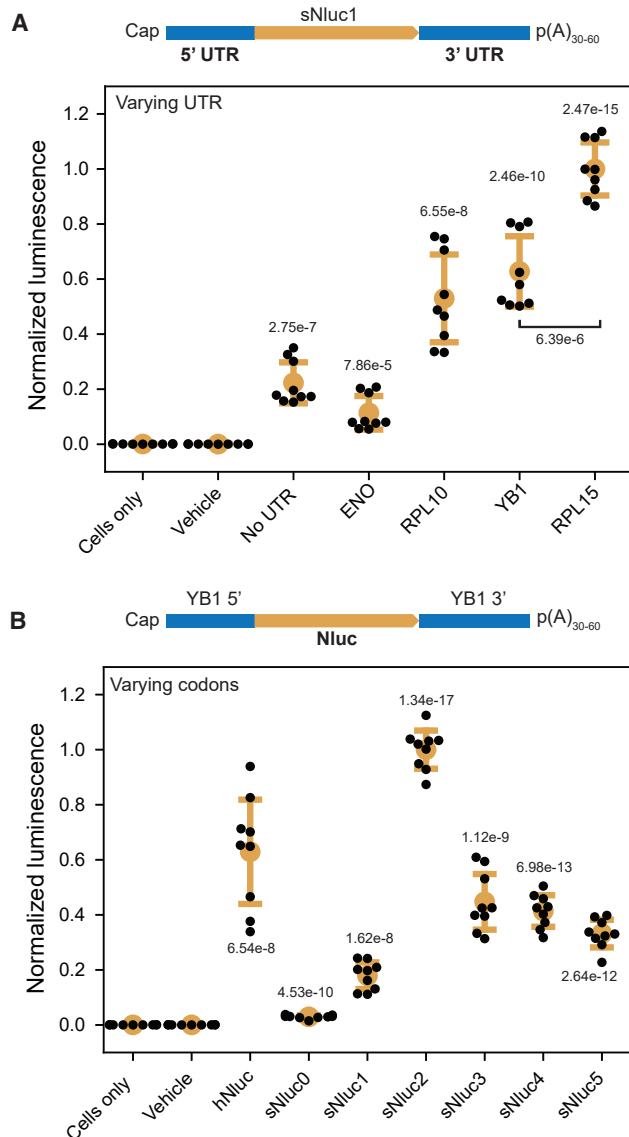
Figure 3. Improving Nluc construct by altering UTR and codon bias

(A) Luminescence from transfections using sNluc1 constructs incorporating different endogenous 5′ and 3′ UTRs, which are identified using gene annotations provided by PlanMine (Rozanski et al., 2019). No-UTR mRNA contains flanking attB1 and attP1 sequences used for cloning. All transfections in this figure are performed with 200,000 cells from whole dissociated planarians using 0.8 μL Viromer and 1 μg mRNA per well and assayed 24 hpt via plate reader.

(B) Luminescence from alternative codon usage variants of Nluc. Codon optimization schemes tested include utilizing the most frequent codon for each amino acid (sNluc0), the IDT online codon optimization tool (sNluc5) with manual adjustments (sNluc1), and random sampling of the codon table biased by the frequency of each codon (sNluc2–4).

Statistics: All data points presented are technical replicates (n = 3) from independent biological replicates (n = 3) using mRNA produced from independent *in vitro* synthesis reactions. Luminescence measurements for each panel are normalized by the mean of the highest intensity construct (A: RPL15; B: sNluc2). Error bars: SDs. ANOVA: p = 4.05 × 10^{-31} (A); p = 2.98e−40 (B). p values reported in the figure are calculated using 2-sided Welch's t test between experimental groups

the rate of translation, we measured the difference between the time when luminescence maximizes (t_{max}) and the time when transfection occurs (t_0) and found that on average, cells reached their maximum luminescence within 60 min after transfection (Figure 4H).

We noticed that the luminescence in individual cells never plateaued, but instead became dimmer after the peak over the course of a few hours, regardless of the transfection time (Figures 4E; Video S2). This phenomenon is unexpected as even if mRNA is rapidly degraded within the cytoplasm, Nluc protein is reported to have a half-life on the order of days in cell lysates (Hall et al., 2012). In addition, Nluc is an ATP-independent luciferase, and therefore should not depend on cell metabolism. We wondered whether the dimming was due to substrate depletion, so we added additional substrate when only a few dimly luminescent cells remained. While some cells recovered partially, most cells remained dark (Figure S6), suggesting that substrate availability was not the only limiting factor. Notably, we occasionally saw cells burst open, releasing Nluc into the media, evident from the single-cell luminescence showing a sudden spike and an immediate drop at the moment of rupture (Figure 4I). However, these events were rare, so cell death was not the major cause of luminescence decay either. These results implied that either planarian cells caused Nluc to be particularly unstable, sequestered, or Nluc was released, actively via secretion or passively through leaky membranes, although the exact mechanism requires further investigation. Together, these results suggest that it is feasible to image Nluc in live cells at high temporal resolution, which provides a powerful tool for quantifying gene expression kinetics in planarian cells.

mRNA transfection can reveal post-transcriptional regulatory elements

The ability to transfect and express exogenous mRNA opens new possibilities for the analysis of gene regulation in planarians. For example, the synthesis of an mRNA and the abundance of its encoded protein can be decoupled by *cis*-acting elements in the UTRs that affect translation or mRNA stability. Understanding which regions of a UTR are responsible for such post-transcriptional regulation requires the ability to remove or add putative regulatory elements to a reporter gene and study how its expression is altered.

As a case study, we selected a transcript (dd_Smed_v6_62_0_1) that contains two long overlapping open reading frames (ORF1: 513 nt, ORF2: 483 nt), with ORF1 beginning 40 nt upstream of ORF2. To resolve which ORF (or both) is translated, we created two constructs with Nluc beginning at the start codon of each ORF. Transfecting these reporters into bulk dissociated cells showed that the translation was specific to ORF1, as Nluc expression was barely detectable from ORF2 (Figure 5A). Removing the start codon of ORF1 by replacing the 5′ UTR with a synthetic sequence (attP1) recovered the Nluc expression. Thus, translation of these transfected RNAs was initiated from the upstream start codon.

and negative controls with cells only, unless specified otherwise in the figure.
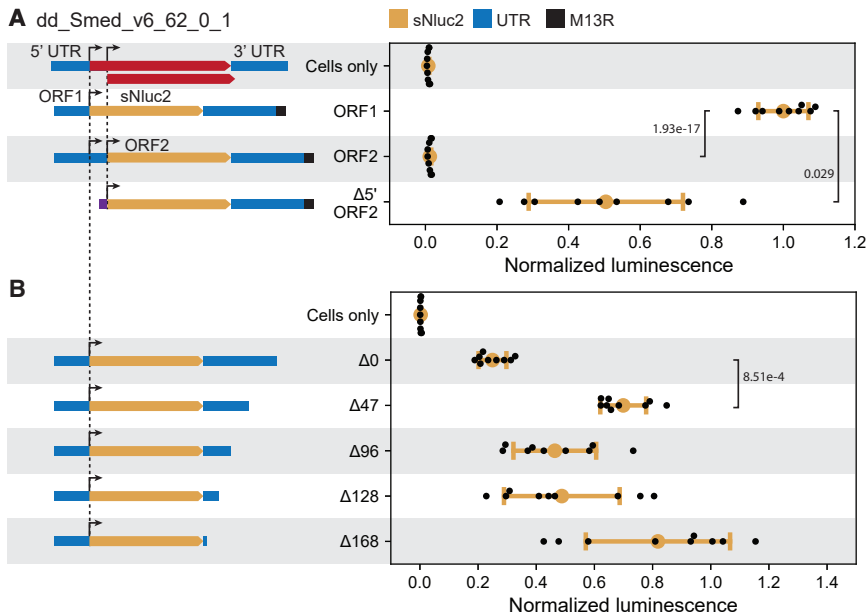
See also Figures S4, S5, and S8.
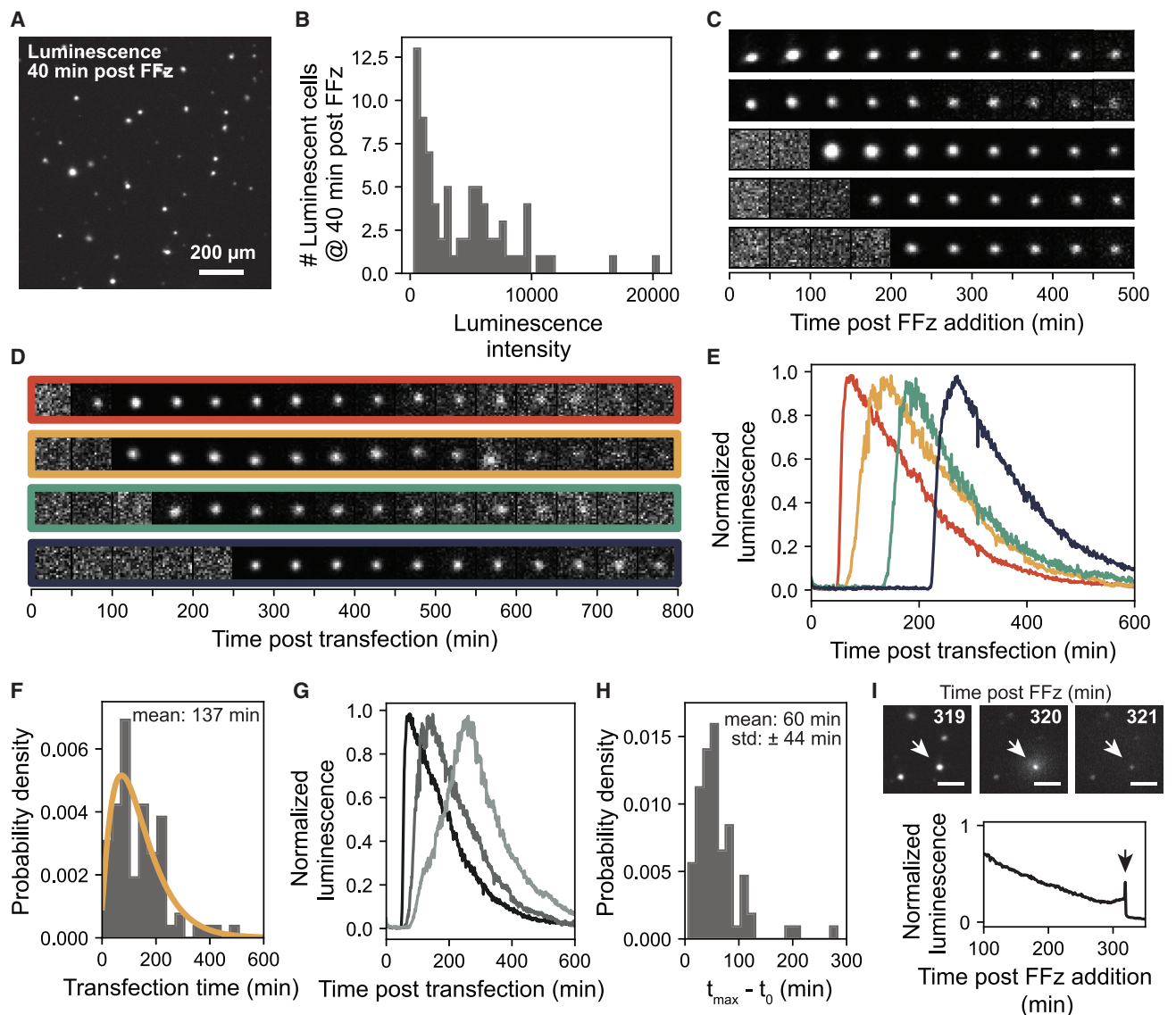
Figure 4. Time-lapse luminescence imaging reveals expression kinetics in single cells

(A) Representative luminescence image of transfected bulk dissociated planarian cells acquired 40 min after FFz addition at 24 hpt.

(B) The distribution of luminescence intensities of single cells.

(C) Examples showing temporal evolution of single-cell luminescence starting at 24 hpt when FFz is added. The 3 cells at the bottom are new transfections during imaging.

(D) Representative images showing luminescence intensity in individual cells. FFz substrate and transfection complexes are added simultaneously at time 0.

(E) Time traces of single-cell luminescence intensities normalized against the maximum intensity of each cell. Luminescence traces correspond to the cell bound by a frame of matching colors in (D).

(F) Distribution of transfection times. Time of transfection is defined as the first time point when the total luminescence intensity of a cell exceeds 3-fold above the background. The curve is fit for a gamma distribution ($\alpha = 2.3$, $\beta = 64.6$).

(G) Example luminescence traces showing individual cells increasing in luminescence at different rates.

(H) Distribution of the time intervals between the time of transfection (t_0) and the time of maximum luminescence (t_{max}).

(I) Images (top) of a transfected cell undergoing cell death and releasing Nluc at 319 mpt (immediately before rupture), 320 mpt (at the moment of rupture), and 321 mpt (after rupture). Scale bars, 100 μm. (Bottom) Normalized luminescence intensity of the cell shown above. The arrow highlights the moment of rupture at 320 mpt.

See also Figure S6 and Videos S1 and S2.

Next, we investigated the function of the 3′ UTR by successively truncating the 3′ UTR from the ORF1 Nluc construct. We found that removing the end of the 3′ UTR, nucleotides 141–188 (Δ47), increased the expression by ∼3-fold, suggesting the presence of a destabilizing or repressing element within this region; deleting additional sequences had minimal additional

effects (Figure 5B). Surprisingly, adding a short synthetic sequence (M13R) to the 3′ end of the full-length UTR drove stronger expression (Figure 5A), implying that the putative repressive or destabilizing element may be sensitive to sequence context. Overall, these results provide a platform for studying post-transcriptional regulation in planarian cells.

Heterologous reporter expression in live animals

Although the ability to transfect planarian cells with mRNA *in vitro* represents a significant advance in the genetic manipulation of planarian cells, current planarian cell culture is limited by low cell viability, lack of cell proliferation, and the gradual loss of neoblast identity (Lei et al., 2019), thus limiting the range of questions that can be addressed in isolated cells. We therefore explored whether our transfection protocols may generate reporter expression in whole animals.

We injected RPL15-sNluc2 mRNA complexed with Viromer or *Trans*IT into the parenchymal tissue along the tail midline, which reduces the risk of misinjections into the abundant gut branches (Figure 6A). We then measured bulk luminescence on individually dissociated animals at multiple time points post-transfection. The luminescence background in tissue lysates from sham-injected animals was very low, mirroring observations *in vitro*. In contrast, transfected tissues exhibited luminescence up to 1,000-fold above background (Figures 6B and 6C). For Viromer, positive animals were already detected at 2 hpt (30/30), and the signal remained robust for 12 hpt (29/30) (Figure 6B). Contrary to *in vitro* conditions, *Trans*IT transfections produced luminescence stronger than that of Viromer transfections by an order of magnitude (Figure 6C), suggesting that *Trans*IT is more effective than Viromer *in vivo*. We next investigated whether luminescence was maintained on a longer timescale. We incubated *Trans*IT-transfected animals for 24–96 h, dissociated the tails (Figure 6D), and used luminescence imaging to distinguish between signals from live cells and extracellular Nluc from dead cells. We

observed luminescent cells up to 96 hpt, although their numbers reduced over time (Figure 6E).

We succeeded in validating Nluc expression using western blotting. Initial efforts using an anti-Nluc antibody failed due to poor binding characteristics. Therefore, we transfected planarians with RPL15-sNluc2 flanked by two 3× FLAG affinity tags. Western blotting using anti-FLAG produced a clear band, providing an orthogonal validation of Nluc expression (Figure 6F). As a comparison, an equivalent mass of transfected HeLa cell lysate was also blotted and produced a significantly brighter signal, consistent with the higher expression measured by luminescence. Together, these results establish mRNA reporter delivery and expression in live planarians.

We next asked whether Nluc expression was sufficient for luminescence imaging *in vivo*. We injected at either the tail midline or behind the left eye. The transfected animals were incubated in NanoGlo-Live substrate supplemented with 1% DMSO to aid in tissue penetration and immobilized to be imaged on an LV200 (Olympus) microscope. This experiment detected luminescence after both Viromer and *Trans*IT injections, while no luminescence was detected in negative controls injected with mRNA alone (Figure S7). Although *in vivo* imaging did not allow for cellular resolution, the size of the luminescent region was consistent with the transfection of a small cluster of cells around the injection site.

Luminescent reporters are particularly attractive for live imaging of planarians, as these animals are agitated by the intense excitation illumination required for fluorescence imaging. Therefore, we tested time-lapse imaging of unrestrained animals and succeeded in tracking luminescence between frames (Figures 6G; Video S3). For these experiments, we used FFz as a low toxicity substrate and found that the animals can be recovered alive after a few hours of imaging. Encouraged by this result, we imaged planarians right after injecting *Trans*IT-mRNA complexes to determine expression kinetics *in vivo*. We further
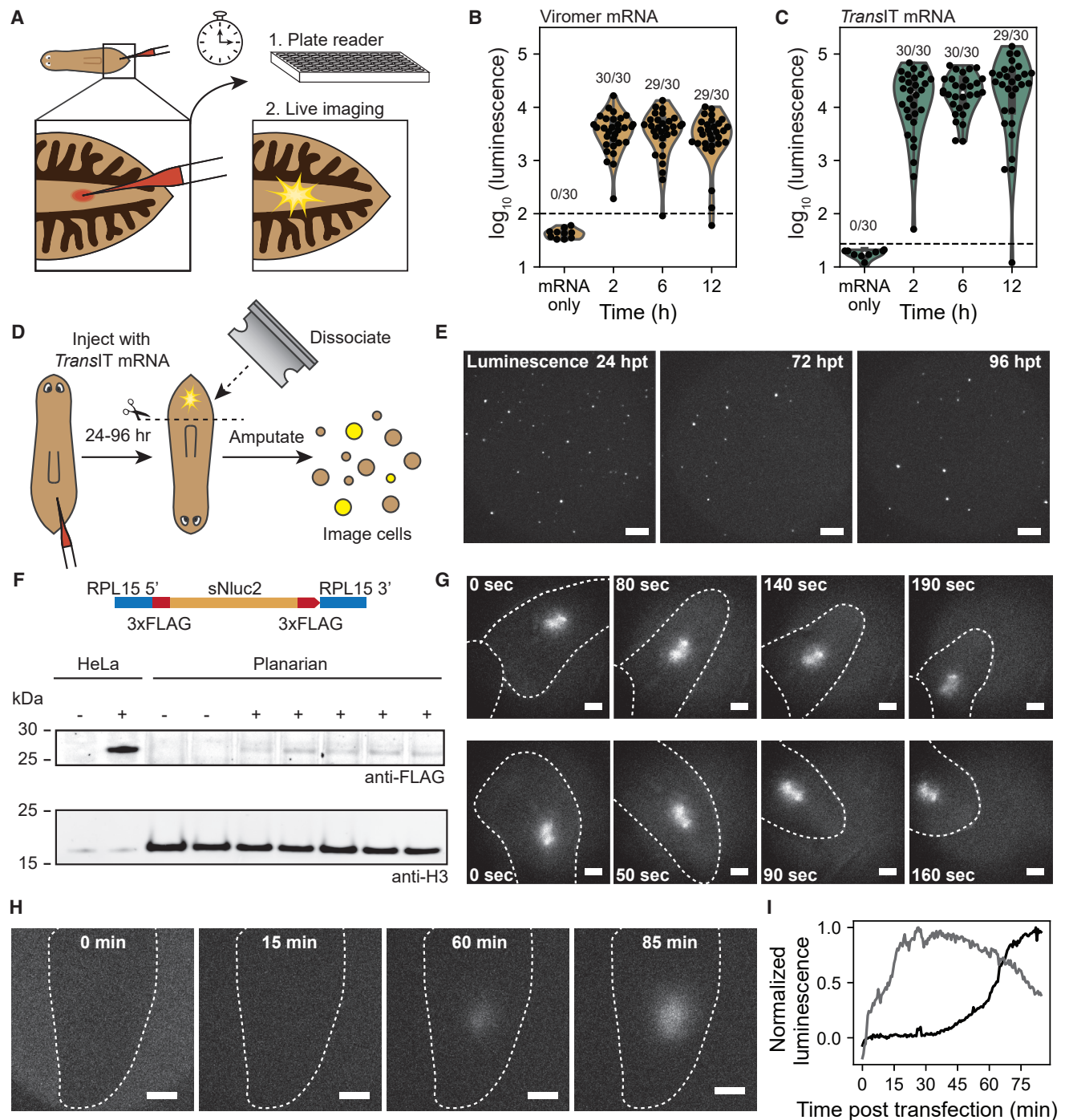
Figure 6. Nluc expression in live animals

(A) Schematics showing the workflow of *in vivo* transfection experiments.

(B and C) Bulk luminescence is measured from dissociated tissues injected with mRNA complexed with Viromer mRNA (B) or *Trans*IT mRNA (C). Dashed lines: 3 standard deviations above the background (based on the mRNA-only condition) to discriminate negatives and positives. Numbers of positive animals out of all animals injected are reported for each time point. Transfected animals are dissociated, and luminescence is measured at room temperature using NanoGlo lysis reagent.

(D) Diagram of luminescence imaging of dissociated tissues from *in vivo* injected animals.

(E) Luminescence images of cells from transfected animals dissociated at 24, 72, and 96 hpt. Five tails are pooled together for dissociation and cells are split evenly into 2–3 concanavalin A-coated 35-mm coverslip bottom dishes. The cells are allowed to settle for 1 h before imaging in Iso-L15 supplemented with 1:250 FFz. Images are acquired using an Andor iXon DU-897 EMCCD with a 20× air objective (BoliOptics, NA = 0.4). Scale bars, 200 μm.

(legend continued on next page)

increased the luminescence signal by injecting the FFz substrate directly into the planarian gut to improve bioavailability and reduce the amount of FFz used per experiment. By continuously imaging for ~1 h, we observed similarly rapid expression kinetics consistent with our observations *in vitro* (Figures 6H and 6I; Video S4). These results represent the first direct measurement of gene expression kinetics in a live planarian, which establishes luminescence as a route for quantitative live imaging through thick, strongly autofluorescent tissues.

DISCUSSION

Transgene expression in planarians has been a challenge in the field since the molecular biology revival of the system 2 decades ago (Agata and Watanabe, 1999; Newmark and Sánchez Alvarado, 2002). Here, we accomplished heterologous protein expression in the planarian model species *S. mediterranea* by combining four experimental approaches: (1) nanostraw electro-delivery to establish an initial positive control, which enabled subsequent optimization of chemical delivery methods; (2) delivering mRNA instead of DNA to bypass the complexities of nuclear import, transcription, and splicing; (3) optimizing post-transcriptional factors to enhance expression; and (4) using a luminescent reporter to circumvent the strong autofluorescence that complicates the use of fluorescent reporters. By making these choices, we observed a clear signal from exogenously supplied Nluc mRNAs in planarian cells both *in vitro* and *in vivo*.

Exogenous reporter expression in our results is supported by multiple independent lines of evidence. First, we showed that most experimental conditions tested reproducibly reached luminescence intensities as high as 3–4 orders of magnitude above the background. Second, we observed that luminescence showed a dose dependence on Nluc mRNA, which was abolished by the addition of a premature stop codon. Third, luminescence intensity was modulated by biologically relevant factors such as UTRs and codon usage bias. Fourth, imaging of transfected cells confirmed the cytoplasmic origin of the luminescence signal, and time-lapse imaging showed rapid expression kinetics in single cells consistent with mRNA expression. Fifth, we succeeded in imaging luminescence in live injected animals, with the signal consistently restricted to the injection site. Sixth, we were able to detect Nluc protein via western blotting from transfected animals. Finally, the results presented in this manuscript were gathered in two laboratories, which highlights the robustness of the technique. Collectively, our results represent the first unambiguous demonstration of exogenous mRNA expression in planarians.

In terms of direct utility, our current reporter assay represents a significant expansion of the planarian toolkit. We demonstrated that by delivering Nluc mRNA, we could identify and optimize transfection methods. New gene delivery strategies are being developed at a rapid pace (Lostalé-Seijo and Montenegro, 2018). Our methodology can be continuously applied to screen this ever-expanding repertoire to achieve more efficient delivery, lower cytotoxicity, and higher expression. Similarly, this approach can be used to assess other mRNA-based expression systems such as self-replicating RNA replicons, including alphavirus (Beal et al., 2015) and nodamuravirus (Taning et al., 2018), which may help to overcome the transient expression of mRNA and increase overall luminescence intensity. Importantly, the use of FFz allowed us to monitor the kinetics of transfection and expression *in vivo* by time-lapse luminescence imaging. This will be valuable for screening DNA-based transgenic methods, as animals may be recovered after luminescence imaging. More broadly, our method also allows testing additional reporters and transfecting other species, with initial success reported in Figures S8A and S8B.

Beyond the technical applications, we demonstrated that Nluc mRNA transfections can be used to study post-transcriptional regulation, an application we anticipate will be of broad interest. This approach provides a route to identify *cis*-regulatory sequences that would have been impossible otherwise. Our method also allows for exploring other post-transcriptional regulatory mechanisms in planarians, such as incorporating *trans*-spliced 5′ leader sequences (Zayas et al., 2005; Rossi et al., 2014), adding target sites of known small RNAs (Kim et al., 2019), including internal ribosomal entry sites (IRES), or manipulating secondary structures of mRNA (Leppek et al., 2022). Our study sets the stage for the systematic characterization and analysis of these factors to better predict how sequence informs expression. In addition to regulatory sequences, the individual nucleotides in mRNA can be modified to increase RNA expression and/or stability (Andries et al., 2015; Svitkin et al., 2017). As a first attempt, we synthesized mRNA containing the uridine analog 1-methyl pseudouridine (m1Ψ) and detected expression in planarian cells (Figure S8C), demonstrating that our method provides a route to explore the regulatory effects of other modified nucleotides.

Limitations of the study
Compared to the current state of the art in established genetic model systems, the absolute level of reporter expression is relatively low in our study. Although this limits the use of fluorescent reporters (given the strong autofluorescence of planarian tissues), we found that Nluc, as a high signal-to-noise reporter,

---

(F) Western blot of Nluc protein from *Trans*IT transfected planarian lysates. Animals are injected along the tail midline and amputated at 12 hpt to collect 3 tails per sample. HeLa cells are transfected with *Trans*IT using the same condition. Top: Schematic diagram of the 6× FLAG-sNluc2 construct.

(G) Snapshots from a time-lapse video of 2 *Trans*IT transfected animals imaged at 4 hpt. Images are collected at 6 frames per min using 10-s exposure time and gain of 500 on an Andor iXon DU-897 EMCCD with a 10× air objective (BoliOptics, NA = 0.25). Animals are decapitated to reduce motility. Dashed lines: animal body boundary. Scale bars, 200 μm.

(H) Expression kinetics of *in vivo* transfection with *Trans*IT. Images show the luminescence intensity before (left) and during (right) expression. Dashed lines: animal body boundary. Scale bars, 200 μm.

(I) Time traces of *in vivo* luminescence from 2 independently injected animals. Luminescence is quantified as the difference between the total intensities from 2 equal-sized regions centered at and above the injection site to subtract out ambient light intensity. The data are normalized by the maximum luminescence. See also Figure S7 and Videos S3 and S4.

allows sensitive and quantitative detection of gene expression. In addition, the chemical transfection reagents were screened and optimized on total cells, which may bias our techniques toward transfecting differentiated cells due to their larger size, higher abundance, and potential lack of post-transcriptional silencing mechanisms. To test this, we developed a method for isolating a highly pure (>95%) population of neoblasts (CRNeoblasts) and found that they showed ~20% luminescence compared to bulk sorted cells after transfection with Viromer (Figures S9A–S9D). However, when we imaged transfected CRNeoblasts, the number of positive cells was <0.02%. Consistently, *in situ* hybridization against a neoblast marker, *piwi-1*, on cells dissociated from animals transfected *in vivo* with *Trans*IT failed to detect convincing cases of Nluc/*piwi-1* co-localization. These results imply that the expression within neoblasts may be very low, delivery may be inefficient, or upon transfection, neoblasts may lose *piwi-1* expression, which is known to be sensitive to the cell cycle (Raz et al., 2021). Efforts need to be made either to identify transfection methods more efficient at transfecting neoblasts, or to better understand how transfection perturbs neoblast identity. Indeed, we observed more luminescent cells from CRNeoblasts transfected via nanostraws, albeit still with a lower efficiency compared to bulk cells (Figure S9E). Finally, Viromer mRNA is no longer commercially available. Since *Trans*IT and Viromer are both cationic polymers, other reagents with similar chemistries may provide substitutes for *in vitro* transfections. For *in vivo* transfections, *Trans*IT is most effective, remains commercially available, and thereby represents the most promising route forward.

STAR★METHODS

Detailed methods are provided in the online version of this paper and include the following:

- KEY RESOURCES TABLE
- RESOURCE AVAILABILITY
  - Lead contact
  - Materials availability
  - Data and code availability
- EXPERIMENTAL MODEL AND SUBJECT DETAILS
  - Planarian models
- METHOD DETAILS
  - Planarian cell dissociation
  - FACS
  - Nanostraw electro-delivery
  - Chemical transfection
  - Luciferase plate assay
  - Luminescence imaging setup
  - Luminescence imaging *in vitro*
  - Luminescence imaging *in vivo*
  - Time-lapse imaging *in vitro*
  - Time-lapse imaging *in vivo*
  - Codon optimization
  - Codon optimization strategies and sequence statistics
  - Cloning
  - *In vitro* transcription
  - Preparation of protein lysates

- SDS-PAGE and immunoblotting
- Single-cell RNA-seq analysis of CRNeoblasts
- QUANTIFICATION AND STATISTICAL ANALYSIS

REFERENCES

Agata, K., and Watanabe, K. (1999). Molecular and cellular aspects of planarian regeneration. Semin. Cell Dev. Biol. *10*, 377–383. https://doi.org/10.1006/scdb.1999.0324.

Aljohani, M.D., El Mouridi, S., Priyadarshini, M., Vargas-Velazquez, A.M., and Frøkjær-Jensen, C. (2020). Engineering rules that minimize germline silencing of transgenes in simple extrachromosomal arrays in C. elegans. Nat. Commun. *11*, 6300. https://doi.org/10.1038/s41467-020-19898-0.

Andries, O., Mc Cafferty, S., De Smedt, S.C., Weiss, R., Sanders, N.N., and Kitada, T. (2015). N1-methylpseudouridine-incorporated mRNA outperforms pseudouridine-incorporated mRNA by providing enhanced protein expression and reduced immunogenicity in mammalian cell lines and mice. J. Control. Release *217*, 337–344. https://doi.org/10.1016/j.jconrel.2015.08.051.

Badr, C.E., Hewett, J.W., Breakefield, X.O., and Tannous, B.A. (2007). A highly sensitive assay for monitoring the secretory pathway and ER Stress. PLoS One *2*, e571. https://doi.org/10.1371/journal.pone.0000571.

Beal, J., Wagner, T.E., Kitada, T., Azizgolshani, O., Parker, J.M., Densmore, D., and Weiss, R. (2015). Model-driven engineering of gene expression from RNA replicons. ACS Synth. Biol. *4*, 48–56. https://doi.org/10.1021/sb500173f.

Benazzi, M., Ballester, R., Baguñá, J., and Puccinelli, I. (1972). The fissiparous race of the planarian dugesia lugubris S.L. found in Barcelona (Spain) belongs to the biotype G: comparative analysis of the karyotypes. Caryologia *25*, 59–68. https://doi.org/10.1080/00087114.1972.10796465.

Böser, A., Drexler, H.C.A., Reuter, H., Schmitz, H., Wu, G., Schöler, H.R., Gentile, L., and Bartscherer, K. (2013). SILAC proteomics of planarians identifies Ncoa5 as a conserved component of pluripotent stem cells. Cell Rep. *5*, 1142–1155. https://doi.org/10.1016/j.celrep.2013.10.035.

Cao, Y., Chen, H., Qiu, R., Hanna, M., Ma, E., Hjort, M., Zhang, A., Lewis, R.S., Wu, J.C., and Melosh, N.A. (2018). Universal intracellular biomolecule delivery with precise dosage control. Sci. Adv. *4*, eaat8131. https://doi.org/10.1126/sciadv.aat8131.

Cardona, A., Hartenstein, V., and Romero, R. (2006). Early embryogenesis of planaria: a cryptic larva feeding on maternal resources. Dev. Genes Evol. *216*, 667–681. https://doi.org/10.1007/s00427-006-0094-3.

Chen, Z.Y., He, C.Y., Ehrhardt, A., and Kay, M.A. (2003). Minicircle DNA vectors devoid of bacterial DNA result in persistent and high-level transgene expression in vivo. Mol. Ther. *8*, 495–500. https://doi.org/10.1016/S1525-0016(03)00168-0.

Collins, J.J., Hou, X., Romanova, E.V., Lambrus, B.G., Miller, C.M., Saberi, A., Sweedler, J.V., and Newmark, P.A. (2010). Genome-wide analyses reveal a role for peptide hormones in planarian germline development. PLoS Biol. *8*, e1000509. https://doi.org/10.1371/journal.pbio.1000509.

Davies, E.L., Lei, K., Seidel, C.W., Kroesen, A.E., McKinney, S.A., Guo, L., Robb, S.M., Ross, E.J., Gotting, K., and Alvarado, A.S. (2017). Embryonic origin of adult stem cells required for tissue homeostasis and regeneration. eLife *6*, e21052. https://doi.org/10.7554/eLife.21052.

Edelstein, A.D., Tsuchida, M.A., Amodaj, N., Pinkard, H., Vale, R.D., and Stuurman, N. (2014). Advanced methods of microscope control using µManager software. J. Biol. Methods *1*, e10. https://doi.org/10.14440/jbm.2014.36.

England, C.G., Ehlerding, E.B., and Cai, W. (2016). NanoLuc: a small luciferase is brightening up the field of bioluminescence. Bioconjug. Chem. *27*, 1175–1187. https://doi.org/10.1021/acs.bioconjchem.6b00112.

Fincher, C.T., Wurtzel, O., de Hoog, T., Kravarik, K.M., and Reddien, P.W. (2018). Cell type transcriptome atlas for the planarian *Schmidtea mediterranea*. Science *360*, eaaq1736. https://doi.org/10.1126/science.aaq1736.

González-Estévez, C., Momose, T., Gehring, W.J., and Saló, E. (2003). Transgenic planarian lines obtained by electroporation using transposon-derived vectors and an eye-specific GFP marker. Proc. Natl. Acad. Sci. USA *100*, 14046–14051. https://doi.org/10.1073/pnas.2335980100.

Grohme, M.A., Schloissnig, S., Rozanski, A., Pippel, M., Young, G.R., Winkler, S., Brandl, H., Henry, I., Dahl, A., Powell, S., et al. (2018). The genome of *Schmidtea mediterranea* and the evolution of core cellular mechanisms. Nature *554*, 56–61. https://doi.org/10.1038/nature25473.

Guo, L., Bloom, J.S., Dols Serrate, D., Boocock, J., Ben David, E., Schubert, O.T., Kozuma, K., Ho, K., Warda, E., Chui, C., et al. (2022). Island-specific evolution of a sex-primed autosome in the planarian. Nature *606*, 329–334. https://doi.org/10.1038/s41586-022-04757-3.

Guo, L., Zhang, S., Rubinstein, B., Ross, E., and Alvarado, A.S. (2016). Widespread maintenance of genome heterozygosity in *Schmidtea mediterranea*. Nat. Ecol. Evol. *1*, 19. https://doi.org/10.1038/s41559-016-0019.

Hall, M.P., Unch, J., Binkowski, B.F., Valley, M.P., Butler, B.L., Wood, M.G., Otto, P., Zimmerman, K., Vidugiris, G., MacHleidt, T., et al. (2012). Engineered luciferase reporter from a deep sea shrimp utilizing a novel imidazopyrazinone substrate. ACS Chem. Biol. *7*, 1848–1857. https://doi.org/10.1021/cb3002478.

Hayashi, T., Asami, M., Higuchi, S., Shibata, N., and Agata, K. (2006). Isolation of planarian X-ray-sensitive stem cells by fluorescence-activated cell sorting. Dev. Growth Differ. *48*, 371–380. https://doi.org/10.1111/j.1440-169X.2006.00876.x.

Jeacock, L., Faria, J., and Horn, D. (2018). Codon usage bias controls mRNA and protein abundance in trypanosomatids. eLife *7*, e32496. https://doi.org/10.7554/eLife.32496.

Kim, T.J., Türkcan, S., and Pratx, G. (2017). Modular low-light microscope for imaging cellular bioluminescence and radioluminescence. Nat. Protoc. *12*, 1055–1076. https://doi.org/10.1038/nprot.2017.008.

Kim, I.V., Duncan, E.M., Ross, E.J., Gorbovytska, V., Nowotarski, S.H., Elliott, S.A., Sánchez Alvarado, A., and Kuhn, C.D. (2019). Planarians recruit piRNAs for mRNA turnover in adult stem cells. Genes Dev. *33*, 1575–1590. https://doi.org/10.1101/gad.322776.118.

Lakshmanan, V., Bansal, D., Kulkarni, J., Poduval, D., Krishna, S., Sasidharan, V., Anand, P., Seshasayee, A., and Palakodeti, D. (2016). Genome-wide analysis of polyadenylation events in *Schmidtea mediterranea*. G3 *6*, 3035–3048. https://doi.org/10.1534/g3.116.031120.

Lei, K., McKinney, S.A., Ross, E.J., Lee, H.C., and Sánchez Alvarado, A. (2019). Cultured pluripotent planarian stem cells retain potency and express proteins from exogenously introduced mRNAs. Preprint at bioRxiv573725. https://doi.org/10.1101/573725.

Leonhardt, C., Schwake, G., Stögbauer, T.R., Rappl, S., Kuhr, J.T., Ligon, T.S., and Rädler, J.O. (2014). Single-cell mRNA transfection studies: delivery, kinetics and statistics by numbers. Nanomedicine. *10*, 679–688. https://doi.org/10.1016/j.nano.2013.11.008.

Leppek, K., Byeon, G.W., Kladwang, W., Wayment-Steele, H.K., Kerr, C.H., Xu, A.F., Kim, D.S., Topkar, V.V., Choe, C., Rothschild, D., et al. (2022). Combinatorial optimization of mRNA structure, stability, and translation for RNA-based therapeutics. Nat. Commun. *13*, 1536. https://doi.org/10.1038/s41467-022-28776-w.

Li, P., Nanes Sarfati, D., Xue, Y., Yu, X., Tarashansky, A.J., Quake, S.R., and Wang, B. (2021). Single-cell analysis of Schistosoma mansoni identifies a conserved genetic program controlling germline stem cell fate. Nat. Commun. *12*, 485. https://doi.org/10.1038/s41467-020-20794-w.

Lim, Y., Shiver, A.L., Khariton, M., Lane, K.M., Ng, K.M., Bray, S.R., Qin, J., Huang, K.C., and Wang, B. (2019). Mechanically resolved imaging of bacteria using expansion microscopy. PLoS Biol. *17*, e3000268. https://doi.org/10.1371/journal.pbio.3000268.

Lostalé-Seijo, I., and Montenegro, J. (2018). Synthetic materials at the forefront of gene delivery. Nat. Rev. Chem *2*, 258–277. https://doi.org/10.1038/s41570-018-0039-1.

Newmark, P.A., and Sánchez Alvarado, A. (2002). Not your father's planarian: a classic model enters the era of functional genomics. Nat. Rev. Genet. *3*, 210–219. https://doi.org/10.1038/nrg759.

Patro, R., Duggal, G., Love, M.I., Irizarry, R.A., and Kingsford, C. (2017). Salmon provides fast and bias-aware quantification of transcript expression. Nat. Methods *14*, 417–419. https://doi.org/10.1038/nmeth.4197.

Plass, M., Solana, J., Wolf, F.A., Ayoub, S., Misios, A., Glažar, P., Obermayer, B., Theis, F.J., Kocks, C., and Rajewsky, N. (2018). Cell type atlas and lineage tree of a whole complex animal by single-cell transcriptomics. Science *360*, eaaq1723. https://doi.org/10.1126/science.aaq1723.

Puigbò, P., Bravo, I.G., and Garcia-Vallve, S. (2008). CAIcal: a combined set of tools to assess codon usage adaptation. Biol. Direct *3*, 38. https://doi.org/10.1186/1745-6150-3-38.

Quax, T.E.F., Claassens, N.J., Söll, D., and van der Oost, J. (2015). Codon bias as a means to fine-tune gene expression. Mol. Cell *59*, 149–161. https://doi.org/10.1016/j.molcel.2015.05.035.

Raz, A.A., Wurtzel, O., and Reddien, P.W. (2021). Planarian stem cells specify fate yet retain potency during the cell cycle. Cell Stem Cell *28*, 1307–1322.e5. https://doi.org/10.1016/j.stem.2021.03.021.

Reddien, P.W. (2018). The cellular and molecular basis for planarian regeneration. Cell *175*, 327–345. https://doi.org/10.1016/j.cell.2018.09.021.

Reddien, P.W., Bermange, A.L., Murfitt, K.J., Jennings, J.R., and Sánchez Alvarado, A. (2005). Identification of genes needed for regeneration, stem cell function, and tissue homeostasis by systematic gene perturbation in planaria. Dev. Cell *8*, 635–649. https://doi.org/10.1016/j.devcel.2005.02.014.

Rink, J.C. (2018). Stem cells, patterning and regeneration in planarians: self-organization at the organismal scale. Methods Mol. Biol. *1774*, 57–172. https://doi.org/10.1007/978-1-4939-7802-1_2.

Rossi, A., Ross, E.J., Jack, A., and Sánchez Alvarado, A. (2014). Molecular cloning and characterization of SL3: a stem cell-specific SL RNA from the planarian *Schmidtea mediterranea*. Gene *533*, 156–167. https://doi.org/10.1016/j.gene.2013.09.101.

Rozanski, A., Moon, H., Brandl, H., Martín-Durán, J.M., Grohme, M.A., Hüttner, K., Bartscherer, K., Henry, I., and Rink, J.C. (2019). PlanMine 3.0 - improvements to a mineable resource of flatworm biology and biodiversity. Nucleic Acids Res. *47*, D812–D820. https://doi.org/10.1093/nar/gky1070.

Sánchez Alvarado, A., and Newmark, P.A. (1999). Double-stranded RNA specifically disrupts gene expression during planarian regeneration. Proc. Natl. Acad. Sci. USA *96*, 5049–5054. https://doi.org/10.1073/pnas.96.9.5049.

Schindelin, J., Arganda-Carreras, I., Frise, E., Kaynig, V., Longair, M., Pietzsch, T., Preibisch, S., Rueden, C., Saalfeld, S., Schmid, B., et al. (2012). Fiji: an open-source platform for biological-image analysis. Nat. Methods *9*, 676–682. https://doi.org/10.1038/nmeth.2019.

Schmiderer, L., Subramaniam, A., Žemaitis, K., Bäckström, A., Yudovich, D., Soboleva, S., Galeev, R., Prinz, C.N., Larsson, J., and Hjort, M. (2020). Efficient and nontoxic biomolecule delivery to primary human hematopoietic stem cells using nanostraws. Proc. Natl. Acad. Sci. USA *117*, 21267–21273. https://doi.org/10.1073/pnas.2001367117.

Sharp, P.M., and Li, W.H. (1987). The codon adaptation index-a measure of directional synonymous codon usage bias, and its potential applications. Nucleic Acids Res. *15*, 1281–1295. https://doi.org/10.1093/nar/15.3.1281.

Su, Y., Walker, J.R., Park, Y., Smith, T.P., Liu, L.X., Hall, M.P., Labanieh, L., Hurst, R., Wang, D.C., Encell, L.P., et al. (2020). Novel NanoLuc substrates enable bright two-population bioluminescence imaging in animals. Nat. Methods *17*, 852–860. https://doi.org/10.1038/s41592-020-0889-6.

Svitkin, Y.V., Cheng, Y.M., Chakraborty, T., Presnyak, V., John, M., and Sonenberg, N. (2017). N1-methyl-pseudouridine in mRNA enhances translation through eIF2α-dependent and independent mechanisms by increasing ribosome density. Nucleic Acids Res. *45*, 6023–6036. https://doi.org/10.1093/nar/gkx135.

Taning, C.N.T., Christiaens, O., Li, X., Swevers, L., Casteels, H., Maes, M., and Smagghe, G. (2018). Engineered flock house virus for targeted gene suppression through RNAi in fruit flies (*Drosophila melanogaster*) *in vitro* and *in vivo*. Front. Physiol. *9*, 805–813. https://doi.org/10.3389/fphys.2018.00805.

Tarashansky, A.J., Xue, Y., Li, P., Quake, S.R., and Wang, B. (2019). Self-assembling manifolds in single-cell RNA sequencing data. eLife *8*, e48994. https://doi.org/10.7554/elife.48994.

Tay, A., and Melosh, N. (2019). Transfection with nanostructure electro-injection is minimally perturbative. Adv. Ther. *2*, 1900133. https://doi.org/10.1002/adtp.201900133.

van der Walt, S., Schönberger, J.L., Nunez-Iglesias, J., Boulogne, F., Warner, J.D., Yager, N., Gouillart, E., and Yu, T.; scikit-image contributors (2014). Scikit-image: image processing in python. PeerJ *2*, e453. https://doi.org/10.7717/peerj.453.

Vila-Farré, M., and C Rink, J. (2018). The ecology of freshwater planarians. Methods Mol. Biol. *1774*, 173–205. https://doi.org/10.1007/978-1-4939-7802-1_3.

Wagner, D.E., Wang, I.E., and Reddien, P.W. (2011). Clonogenic neoblasts are pluripotent adult stem cells that underlie planarian regeneration. Science *332*, 811–816. https://doi.org/10.1126/science.1203983.

Xie, X., Xu, A.M., Leal-Ortiz, S., Cao, Y., Garner, C.C., and Melosh, N.A. (2013). Nanostraw-electroporation system for highly efficient intracellular delivery and transfection. ACS Nano *7*, 4351–4358. https://doi.org/10.1021/nn400874a.

Zayas, R.M., Bold, T.D., and Newmark, P.A. (2005). Spliced-leader trans-splicing in freshwater planarians. Mol. Biol. Evol. *22*, 2048–2054. https://doi.org/10.1093/molbev/msi200.

Zeng, A., Li, H., Guo, L., Gao, X., McKinney, S., Wang, Y., Yu, Z., Park, J., Semerad, C., Ross, E., et al. (2018). Prospectively isolated tetraspanin[+] neoblasts are adult pluripotent stem cells underlying planaria regeneration. Cell *173*, 1593–1608.e20. https://doi.org/10.1016/j.cell.2018.05.006.

STAR★METHODS

KEY RESOURCES TABLE

REAGENT or RESOURCE	SOURCE	IDENTIFIER
Antibodies		
Mouse anti-FLAG M2	Merck	Cat#F3165, RRID:AB_259529
Rabbit anti-Histone H3	Abcam	Cat#ab1791, RRID:AB_302613
Goat anti-mouse-CF770	Biotium	Cat#20077, RRID: AB_10852670
Goat anti-rabbit-CF680	Biotium	Cat#20067, RRID: AB_10871686
Chemicals, peptides, and recombinant proteins		
Hoechst 33342 (10 mg/mL)	ThermoFisher	Cat#H3570
Calcein AM (1 mg)	ThermoFisher	Cat#C1430
CellRox Green (2.5 mM)	Invitrogen	Cat#C10444
LysoTracker Deep Red (1 mM)	Invitrogen	Cat#L12492
BsaI-HF®v2	NEB	Cat#R3733S
BbsI-HF	NEB	Cat#R3539S
T4 DNA Ligase	NEB	Cat#M0202S
Pseudouridine-5′-Triphosphate	Tri-Link	Cat#N-1019-1
Concanavalin A	Millipore Sigma	Cat#L7647-25MG
Instant Ocean	Carolina Biological Supply	Cat#671442
Leibovitz's L-15 Media	ThermoFisher	Cat#11415064
Ciprofloxacin HCl	Millipore Sigma	Cat#PHR1044-1G
MEM Non-essential Amino Acids Solution (100X)	ThermoFisher	Cat#11140076
Antibiotic-Antimycotic (100X)	ThermoFisher	Cat#15240062
MEM Vitamin Solution (100X)	ThermoFisher	Cat#11120052
Sodium Pyruvate (100 mM)	ThermoFisher	Cat#11360070
UltraPure Low Melting Point Agarose	ThermoFisher	Cat#16520050
Linalool, 97%	Millipore Sigma	Cat#L2602-5G
1,1,1-Trichloro-2-methyl-2-propanol hemihydrate (chloretone), 98%	Millipore Sigma	Cat# 112,054-50G
Soy Protein Isolate	Powerstar Food	Cat#psf-1131
1× MOPS	ThermoFisher	Cat#NP0001
Critical commercial assays		
T7 mScript™ Standard mRNA Production System	CELLSCRIPT	Cat#C-MSC100625
Nano-Glo® Luciferase Assay System, Furimazine	Promega	Cat#N1110
Nano-Glo® Live Cell Assay System, Furimazine	Promega	Cat#N2011
Nano-Glo® In Vivo Substrate, Fluorofurimazine	Promega	Cat#CS320501
DNA Clean & Concentrator-5	Zymo Research	Cat#D4004
TransIT®-mRNA Transfection Kit	Mirus Bio	Cat#MIR 2225
Viromer® mRNA	Lipocalyx	N/A
Viromer® RED	Lipocalyx	N/A
Viromer® GREEN	Lipocalyx	N/A
RmesFect	OZ Biosciences	Cat#RM20500
Lipofectamine™ 3000	ThermoFisher	Cat#L3000001
INTERFERin	Polyplus	Cat#101000036
RNAiMax	ThermoFisher	Cat#13778100
FuGENE® HD	Promega	Cat#E2311
Phusion High-Fidelity PCR Master Mix with HF Buffer	ThermoFisher	Cat#F531L
Pierce™ Gaussia Luciferase Glow Assay Kit	ThermoFisher	Cat#16160

(Continued on next page)

Continued

REAGENT or RESOURCE	SOURCE	IDENTIFIER
Deposited data		
CRNeoblast single-cell RNAseq	This paper	NCBI BioProject: PRJNA863273
Experimental models: organisms/strains		
Schmidtea mediterranea (sexual)	N/A	N/A
Schmidtea mediterranea (asexual)	N/A	CIW4
Schmidtea polychroa	N/A	Spol55
Schmidtea polychroa	N/A	Spol200
Oligonucleotides		
Primers used in this study	This paper	See Table S1
Recombinant DNA		
pNHT7	This paper	Addgene#186753
pEXPR_pGAPDH::sNluc1::tGAPDH	This paper	Addgene#187221
pEXPR_pGAPDH::H2B-smed-mScarlet::tGAPDH	This paper	Addgene#186764
pNHT7::ENO::sNluc1	This paper	Addgene#186755
pNHT7::RPL15::sNluc1	This paper	Addgene#186757
pNHT7::RPL10::sNluc1	This paper	Addgene#186756
pNHT7::YB1::sNluc1	This paper	Addgene#186754
pNHT7::YB1::hNluc	This paper	Addgene#186774
pNHT7::YB1::sNluc0	This paper	Addgene#186758
pNHT7::YB1::sNluc2	This paper	Addgene#186759
pNHT7::YB1::sNluc3	This paper	Addgene#186760
pNHT7::YB1::sNluc4	This paper	Addgene#186761
pNHT7::YB1::sNluc5	This paper	Addgene#186762
pNHT7::ENO::sNluc2	This paper	Addgene#186770
pNHT7::RPL15::sNluc2	This paper	Addgene#186763
pNHT7::RPL15::sNluc0	This paper	Addgene#186771
pNHT7::RPL15::hNluc	This paper	Addgene#186772
pNHT7::UMSBP::sNluc2_ORF1	This paper	Addgene#186765
pNHT7::UMSBP::sNluc2_ORF2	This paper	Addgene#186766
pNHT7::RPL15::hGluc	This paper	Addgene#186768
pNHT7::RPL15::sGluc	This paper	Addgene#186769
pNHT7::RPL15-sNluc2_STOP	This paper	Addgene#186767
Software and algorithms		
Fiji	(Schindelin et al., 2012)	https://imagej.net/software/fiji/#downloads
Gen 5™	BioTek	https://www.biotek.com/products/software-robotics-software/gen5-microplate-reader-and-imager-software/
Scikit-image	(van der Walt et al., 2014)	https://scikit-image.org/
scanR Analysis 3.2.0	Olympus	
Micromanager 1.4	(Edelstein et al., 2014)	https://micro-manager.org/Download_Micro-Manager_Latest_Release
Salmon v1.4.0	(Patro et al., 2017)	https://combine-lab.github.io/salmon/
SAM v0.8.1	(Tarashansky et al., 2019)	https://github.com/atarashansky/self-assembling-manifold
Other		
Sony SH800 Cytometer	Sony	N/A
Sony Cell Sorting Chip (100 μm)	Sony	Cat#LE-C3210
BioTek HTX Synergy	BioTek	Cat#S1LFA
BioTek Synergy™ *Neo2*	BioTek	N/A

(Continued on next page)

Continued

REAGENT or RESOURCE	SOURCE	IDENTIFIER
EnVision Microplate Reader	PerkinElmer	N/A
Olympus LV200	Olympus	N/A
FluoroDish Cell Culture Dish (35 mm)	WPI	Cat#FD3510-100
Sutter P-97 Needle Puller	Sutter	Cat#P-97
XenoWorks Digital Microinjector	Sutter	Cat#BRE
Borosilicate Glass Capillary (1 mm OD, with filament)	WPI	Cat#1B100F3
Nanostraw Cartridges	NAVAN Technologies	N/A
Nav400	NAVAN Technologies	N/A
XCell SureLock Mini-Cell and XCell II System	Invitrogen	Cat#EI0002
NuPAGE 4-20% BisTris Gel	ThermoFisher	Cat#NP0321BOX
0.45 μm Nitrocellulose Membrane	Millipore Sigma	Cat#GE10600002
Amersham Typhoon	Cytiva	N/A

RESOURCE AVAILABILITY

Lead contact
Further information and requests for resources and reagents should be directed toward the lead contact, Bo Wang (wangbo@stanford.edu).

Materials availability
Plasmids used in this study are available freely upon request and have been deposited to Addgene (#186753-#186774, and #187221). Though no longer commercially available, Viromer mRNA is available upon request while our limited supplies last. Nanostraw electro-delivery is presently being commercialized by NAVAN Technologies, who can be reached for inquiry. All species and strains of planarians used in this study are available upon request.

Data and code availability
- Raw and processed single-cell RNAseq dataset generated for this study are available from NCBI BioProject with an accession number PRJNA863273.
- This paper does not report any original code.
- Any additional information required to reanalyze the data reported in this paper is available from the lead contact upon request.

EXPERIMENTAL MODEL AND SUBJECT DETAILS

Planarian models
Asexual *S. mediterranea* strain CIW4 were reared in the dark at 20°C and maintained in 0.5 g/L Instant Ocean (Carolina Biological Supply, Cat#671442) supplemented with 0.1 g/L sodium bicarbonate and were fed a diet of macerated calf liver once per week. *Schmidtea polychroa* strains were reared in the dark at 20°C and maintained in 0.75× Montjuic Salts (1.2 mM NaCl, 0.75 mM CaCl$_2$, 0.75 mM MgSO$_4$, 0.075 mM MgCl$_2$, 0.075 mM KCl) supplemented with 0.1 g/L sodium bicarbonate and were fed a diet of macerated calf liver once per week.

METHOD DETAILS

Planarian cell dissociation
Planarian cells were prepared by finely mincing 10-15 asexual *S. mediterranea* (5-7 mm in length) with a razor blade and suspending the tissue in CMF (Ca/Mg-Free media: 480 mg/L NaH$_2$PO$_4$, 960 mg/L NaCl, 1.44 g/L KCl, 960 mg/L NaHCO$_3$, 3.57 g/L HEPES, 0.24 g/L D-glucose, 1 g/L BSA, pH 7.4 in MilliQ H$_2$O). The tissue was rocked for 5 min, followed by gentle pipetting for 10 min for 3 times, or until the tissue was visibly homogenized. The cells were centrifuged at 250 g for 4 min, and the supernatant was removed and replaced with 1.5 mL of fresh CMF. The cell suspension was then serially filtered through 100, 70, 40, and 35-μm mesh strainers. The filtered cell suspension was centrifuged and transferred to Iso-L15 (1:1 Leibovitz's L-15 to MilliQ H$_2$O, 1× MEM non-essential amino acids, 1× antibiotic-antimycotic, 1× MEM vitamin solution, 1 mM Sodium Pyruvate, 2.5 g/L HEPES, 5% FBS, buffer to pH 7.8).

FACS

To isolate the X1FS population, an aliquot of sacrificial cells was stained with Hoechst 33342 (10 μg/mL, ThermoFisher, Cat#H3570) in CMF for 15 min, filtered, and sorted on a Sony SH800 with either the 100 or 130 μm sorting chip (Sony, Cat#LE-C3210, Cat#LE-C3213). Cells were gated for size using forward and side-scatter signals, then neoblasts were identified by gating, in linear scale, on cells with high Hoechst blue (Excitation: 405 nm, Emission 450/50 nm) and low Hoechst red (Excitation: 405 nm, Emission 600/60 nm) signal (Hayashi et al., 2006). Following the identification of the neoblast population using Hoechst fluorescence, unstained planarian cells were loaded and sorted into Iso-L15 medium using the X1FS gate overlaid on the forward and side-scatter. After sorting, the cells were centrifuged at 250 g for 5 min and resuspended in fresh Iso-L15.

To isolate CRNeoblasts, dissociated cells at a density of 1-5×10^6 cells/mL were stained with 1:500 (5 μM) CellRox Green (Invitrogen, Cat# C10444) and 1:7000 (143 nM) LysoTracker Deep Red (Invitrogen, Cat# L12492). The sample was rocked gently in the dark for 30 min at room temperature. After incubation, the cells were pipetted up and down before being strained through a 35 μm filter cap FACS tube. The cells were sorted on a Sony SH800 with a 100 μm sorting chip. Cells were first gated by forward and side-scatter, then a final gate around CellRox Green high and LysoTracker Deep Red low identified the CRNeoblast population (Figure S9A).

Nanostraw electro-delivery

Nanostraws were acquired from NAVAN Technologies. Each nanostraw cartridge was loaded with 200,000 X1FS cells in 300 μL of Iso-L15 media and centrifuged at 300 g for 10 min to ensure close contact between straws and cells. For each cartridge, 3 μg of *in vitro* synthesized mRNA was diluted in PBS to a total volume of 35 μL and placed on the titanium anode, and a cartridge was carefully lowered onto the mRNA solution. The titanium cathode was placed atop, and the electro-delivery assembly was subjected to a 35 V, 200 μs, 40 Hz square wave pulse 3 times for 45 s each, with a 1 min rest in between pulses. Transfected cells were incubated at 20°C in the dark for 24 h before being transferred from the nanostraw cartridge to an opaque white 96 well plate (Greiner, Cat#655075) for assaying luminescence.

Chemical transfection

For *in vitro* experiments, dissociated planarian cells were suspended at a concentration of 0.88×10^6 cells/mL in Iso-L15 medium supplemented with 10 μg/mL ciprofloxacin (Sigma-Aldrich, Cat#PHR1044). 225 μL of cell suspension was added to each well of white opaque (for plate-reader assays) or glass bottom (for luminescence imaging) 96-well plates for a total of ∼200,000 cells per well. For the initial screen, each reagent was prepared as specified in Table S2, and for all subsequent experiments, we utilized the optimal reagent ratios identified in Figures 2C and 2D. After adding transfection complexes to each well, the cells were incubated at 20°C in the dark for 4-72 h before assaying luminescence. Biological replicates were performed by transfecting independently synthesized batches of mRNA, dissociated planarian cells, and assembled transfection complexes. Within each biological replicate, transfection mixes were split evenly across 3 parallel transfections of cells isolated from the same dissociation.

For live animal transfections, either 0.8 μL of Viromer, 1 μg of RPL15-sNluc2 mRNA, and Viromer Buffer were added to a final reaction volume of 25 μL, or 2 μL of *Trans*-IT, 1 μL of Boost, 1.5 μg of RPL15-sNluc2 mRNA, up to a final volume of 25 μL in serum-free L-15. Viromer and *Trans*-IT complexes were allowed to incubate at room temperature for 15 and 5 min, respectively, prior to being loaded into needles pulled from glass capillaries (WPI, Cat#1B00F-3) on a Sutter P97 needle puller with the following settings: pressure = 500, heat = 758, pull = 50, velocity = 70, time = 200. Needles were loaded on a FemtoJet injection system (Eppendorf) or Sutter XenoWorks injection system, and the needle tip was opened with forceps. Animals were placed ventral-side up on moist filter paper placed on a cooled block. Animals were injected along the tail midline with 900 nL transfection mix or until a bolus of injected fluid was visible and ceased expanding. For ocular injections, animals were placed ventral-side down and injected immediately posterior to the left eye cup. Animals were left to rest in the dark at 20°C until assaying 4-24 hpt.

Luciferase plate assay

For dissociated cells, luminescence was measured using the NanoGlo-Live Cell Assay (Promega, Cat# N2011). NanoGlo-Live substrate was added to NanoGlo buffer at a ratio of 1:20, and 25 μL of reagent was added to 250 μL of transfected cells. NanoGlo-Live reagent was also added to negative control conditions before assaying to ensure a consistent luminescence baseline.

For live planarians, each injected animal was individually dissociated by finely mincing with a razor blade and suspending the tissue in 250 μL Iso-L15 medium just prior to assaying. The resuspended tissue was transferred to an opaque white 96-well plate. Nluc expression was measured using the NanoGlo Luciferase Assay System (Promega, Cat# N1110). Substrate was added to the NanoGlo lysis buffer at a ratio of 1:50 and 100 μL of reagent was added to the cells. Cells were lysed by pipetting up and down 10 times or until the tissue was visibly homogenized.

Gaussia luciferase (Gluc) was assayed using the Pierce Gaussia Luciferase Glow Assay Kit (ThermoFisher, Cat#16160) according to the manufacturer's instructions. To measure luminescence from supernatant and cellular pellets, 250 μL of supernatant was carefully transferred to a fresh 96-well plate, then the remaining cells were resuspended in 250 uL of CMF. The resuspended cells were then transferred to a fresh 1.5 mL Eppendorf tube and were centrifuged at 250 g for 4 min. The supernatant was discarded, and the cells were then resuspended in 250 μL of Iso-L15 and transferred to an opaque white 96-well plate.

Luminescence was measured on a plate reader (BioTek Synergy HTX for collecting data presented in Figures 1, 3, 5, S2, S5, S8, S9; BioTek Synergy *Neo*2 for Figures 2C and 2D, 6B, 6C, S2; and EnVision Microplate Reader for Figure 2B). Integration time was set at 1 s and the digital gain was kept consistent on each instrument for all experiments. All assays were performed at room temperature and luminescence was measured quickly after substrate was added to all wells.

Luminescence imaging setup

Luminescence imaging was performed on an LV200 Bioluminescence Imaging System (Olympus) equipped with a 20× air objective (Olympus: UPLXAPO20×, N.A. = 0.8), a 60× oil immersion objective (Olympus: UPLXCAPO60XO, N.A. = 1.42), and a liquid-cooled Hamamatsu C9100-24B EMCCD camera (1024 × 1024 pixels). All images taken with the LV200 were acquired with an exposure of 60 s and a gain of 300 unless otherwise specified.

Images were also acquired with a custom-built luminescence microscope, modified from Kim et al. (2017), which utilizes an Andor iXon DU-897 EMCCD camera (512 × 512 pixels), a HIKROBOT MVL-HF5024M-10MP 50mm tube lens, and either a 10× air (BoliOptics: BM13013331, N.A. = 0.25), a 20× air (BoliOptics: BM03023431, N.A. = 0.4), or a 100× oil (Carl Zeiss: 1084–514, N.A. = 1.45) objective. All images taken with the custom luminescence microscope were acquired with an exposure time of 30 s and gain of 500 unless otherwise specified. Micromanager 1.4 was used to operate the microscope.

Luminescence imaging *in vitro*

Nluc expression was detected using the NanoGlo-Live Cell Assay. A 35 mm glass-bottom dish (WPI, Cat#FD3510-100) or a glass bottom 96-well plate (Cellvis, Cat#P96-1-N) were coated with 0.5 mg/mL Concanavalin A (Sigma-Aldrich, Cat# L7647) for 2 h, washed, and air dried. Transfected cells were transferred to coated dishes in a total of 250 μL of Iso-L15 and allowed to adhere to the glass surface for 1 h to prevent cells from moving in and out of the imaging plane. NanoGlo-Live substrate was added to NanoGlo buffer at a ratio of 1:20, and 25 μL of reagent was added to 250 μL of transfected cells. Cells were imaged at room temperature with either an LV200 Bioluminescence Imaging System (Olympus) with a 60× oil immersion objective (Olympus UPLXCAPO60XO), or the custom-built luminescence microscope equipped with a 100× oil immersion objective (Carl Zeiss, 1084-514).

Quantification of transfection efficiency and viability were measured by staining transfected cells with Calcein AM (1 μM final concentration), propidium iodide (PI) (1 μg/μL final concentration), and Hoechst 33342 (1 μg/μL final concentration). The cells were imaged on an LV200 with a 20× air objective (Olympus), and individual cells were classified using scanR Analysis 3.2.0 (Olympus). Transfected cells were classified as being positive for Calcein, Hoechst, and Nluc. Viability was quantified by classifying live cells as positive for both Calcein and Hoechst. Total cells were quantified by Hoechst positive nuclei.

Luminescence imaging *in vivo*

For *in vivo* imaging, animals were incubated in 100 μL of 1× Instant Ocean supplemented with 1% DMSO and 1:20 NanoGlo-Live substrate for 15 min at room temperature. The animals were then placed on glass bottom dishes cooled on ice. Excess water was wicked away, and the animals were embedded in 1.5-2% low-melt agarose gel (ThermoFisher, Cat#16520050) supplemented with 1:5000 linalool (Sigma-Aldrich, Cat#L2602) and 1:20 NanoGlo-Live substrate. A coverslip was placed over the agarose to prevent lensing. The animals were imaged using an LV200 with a 20× air objective (Olympus) at an exposure of 60 s and gain of 300.

Time-lapse imaging *in vitro*

Bulk dissociated planarian cells were transfected with 0.8 μL of Viromer and 1 μg RPL15-sNluc2 mRNA. Cells were either imaged immediately or allowed to incubate for 24 h at 20°C. Substrate was prepared by diluting NanoGlo In-Vivo substrate (FFz) (Promega, Cat#CS320501) 1:50 in Iso-L15, then 25 μL of this solution was added to the 250 μL of transfected cell media. Cells were imaged at room temperature on a custom-built luminescence microscope with a 20× air objective (BoliOptics, N.A. = 0.4) at 1 frame per min with an exposure of 30 s and gain of 500. Individual cells were automatically segmented using Python 3.8 and scikit-image.

Time-lapse imaging *in vivo*

To image unrestrained animals, they were allowed to incubate at 20°C for 4 h post injection, then amputated immediately anterior to the injection site. The animals were placed in a solution of 1× Instant Ocean containing 1:20 NanoGlo In-Vivo substrate (FFz) and imaged at a rate of 6 frames per min with an exposure of 10 s and gain of 500.

For measuring expression kinetics *in vivo*, animals were allowed to rest for 15 min post injection and re-mounted ventral-side up on moist filter paper over a cool block. Undiluted FFz was injected into the gut until at least one posterior gut branch had visibly filled with yellow substrate, then the animal was placed ventral-side down on a cooled glass-bottom dish. Excess water was wicked away before immobilization. Anesthetic agarose was prepared by mixing 2% agarose in 1% chloretone (Sigma-Aldrich Cat# 112,054) dissolved in 1× Instant Ocean supplemented with 1:5000 linalool. The agarose solution was cooled to 37°C and allowed to cool further just before gelation began, and drops were added on and around the animal to immobilize it. Animals were imaged at room temperature on a custom-built luminescence microscope with a 10× air objective (BoliOptics, N.A. = 0.25) at 2 frames per min with an exposure of 30 s and gain of 500.

Codon optimization

Coding sequences were codon optimized using three approaches: (1) IDT: codons were chosen based on IDT's online codon optimization tool, (2) Most frequent: utilizing only the most frequently observed codon according to the *S. mediterranea* codon usage table (http://www.kazusa.or.jp/codon/), (3) Biased sampling: probabilistic sampling of codons weighted by their frequency in the *S. mediterranea* codon usage table. The codon adaptation index (CAI) of each gene was calculated using an online CAI calculator (https://ppuigbo.me/programs/CAIcal). All sequences are available through Addgene (see STAR Methods).

Codon optimization strategies and sequence statistics

Sequence name	Optimization method	%GC	CAI
smed-mScarlet	IDT	32.6%	0.891
smed-H2B-mScarlet	IDT	33.7%	0.866
hNluc	None	52.7%	0.485
sNluc0	Most frequent	27.1%	1.0
sNluc1	IDT	29.8%	0.925
sNluc2	Biased sampling	38.4%	0.713
sNluc3	Biased sampling	40.1%	0.663
sNluc4	Biased sampling	36.4%	0.743
sNluc5	IDT	40.9%	0.633
sGluc	Biased sampling	40.7%	0.745
hGluc	None	58.6%	0.441

Cloning

To generate a plasmid for *in vitro* transcription and harvesting the UTR sequences, we first amplified the backbone of pDONOR221 (ThermoFisher, Cat#12536017) using primers BW-NH-104-105 (all primer sequences are provided in Table S1), as well as the LacZ cassette from pUC19 (Addgene #50005) with a T7 promoter sequence followed by a BsaI restriction site for subsequent cloning steps, all flanked between BbsI restriction sites and M13 forward and M13 reverse primer sites (for *in vitro* transcription template production) using primers BW-NH-106-107. The amplified backbone was digested with BsaI-HFv2 (NEB, Cat#R3733S) and the LacZ insert was digested with BbsI-HF (NEB, Cat#R3539S). The digested backbones were purified using the Zymo Clean and Concentrate kit (Zymo, Cat#D4004). The purified fragments were ligated together using T4 DNA Ligase (NEB, Cat#M0202S) to create pNHT7 (Figure S4A).

We cloned the gene of interest (GOI) from a pool of planarian cDNA using primers (BW-NH-108-125) containing BsaI restriction sites to produce overhangs compatible with pNHT7. The amplicons were purified using the Zymo Clean and Concentrate kit and then inserted into pNHT7 via a golden gate reaction containing 40 ng of backbone and 20 ng for each insert to be cloned in a 20 μL reaction volume containing 2 μL T4 Ligase Buffer, 1 μL T4 DNA Ligase, and 1 μL BsaI-HFv2 to produce pNHT7:GOI (Figure S4B).

Finally, to insert a reporter between the 5′ and 3′ UTRs, we amplified pNHT7:GOI with outward facing primers (BW-NH-128-139) which bind to the end and beginning of the 5′ and 3′ UTRs respectively containing the BsaI restriction sites. The reporter was then amplified to append compatible BsaI restriction sites using primers BW-NH-174-185 and inserted between the two UTR sequences via a golden gate reaction. The resulting plasmids were amplified with M13 forward and M13 reverse primers to produce linear template for *in vitro* transcription reactions (Figure S4C).

In vitro transcription

Linearized templates for *in vitro* transcription were amplified using Phusion Polymerase (ThermoFisher, Cat#F531L) in two parallel 50 μL format reactions containing 10 μM M13 F/R primers (Table S1) and 25 ng of template DNA. The two reactions were pooled and purified using the Zymo Clean and Concentrator kit, and the templates were eluted in 8 μL of RNase-free water. For the 'UTR hacking' experiments (Figure 5), PCRs were performed as described but replacing the M13R primer for an oligo which primes directly to the 3′ UTR (Table S1). Expected concentrations should range from 200-300 ng/μL.

In vitro transcription (IVT) was performed using the T7 mScript Standard mRNA Production System (CELLSCRIPT, Cat#C-MSC100625) according to the manufacturer's protocol, opting for a 1.5 h incubation during T7 transcription, a 2 h incubation for 5′ capping, and a 1 h incubation for poly-A tailing, all performed at 37°C. RNA purification was performed by adding 600 μL of ethanol and 50 μL of 10 M ammonium acetate to 200 μL of IVT reaction, and allowing to precipitate overnight at −20°C. The precipitated mRNA is then centrifuged at 21,000 g for 30 min at 4°C. The pellet was then rinsed twice with 70% ethanol and allowed to air dry before being resuspended in 60 μL of nuclease-free water. A standard 60 μL reaction typically yields 60 μg of mRNA. For expected

results, see Figures S5A–S5C. For mRNA containing m1Ψ, the rNTP mix provided in the CELLSCRIPT kit was substituted for a mixture of rNTPs containing 10 mM rGTP, 10 mM rCTP, 10 mM rATP, and 10 mM m1Ψ (Tri-Link, Cat#N-1019-1). The IVT reaction can be scaled down by a half, though precipitation was done with the full volumes described here.

Preparation of protein lysates

At 12 hpt, animals were washed twice with 1× Instant Ocean and decapitated to enrich for the injected regions. Three tails were pooled for each sample, transferred to a 1.5 mL tube and 80 μL Urea lysis buffer (9 M Urea, 100 mM NaH_2PO_4, 10 mM Tris-Base, 2% w/v SDS, 130 mM DTT, 1mM $MgCl_2$) was added. Animals were immediately lysed with a motorized pestle, followed by incubation at room temperature for 20 min to fully denature proteins. Cellular debris was then pelleted by centrifugation at 21,000 g for 15 min and supernatant was moved to a fresh 1.5 mL tube. Small aliquots from the protein lysates were diluted 1:10 in MilliQ H_2O to quantify protein concentration based on 280 nm absorbance using a spectrophotometer. 20 μL of 5× LDS buffer (530 mM Tris HCl, 700 mM Tris-Base, 10% w/v LDS, 50% w/v glycerol, 2.55 mM EDTA, 500 mM DTT, 0.11 mM SERVA Blue G250, 0.875 mM Phenol Red, pH 8.5) was then added to each sample.

SDS-PAGE and immunoblotting

SDS-PAGE and Western blotting were performed using a XCell SureLock Mini-Cell and XCell II system (Invitrogen, Cat#EI0002). 40 μg total protein from planarian lysate or 5 μg total protein from HeLa cell lysate was loaded per well onto a NuPAGE 4-20% BisTris gel (ThermoFisher, Cat#NP0321BOX) and run in 1× MOPS buffer (ThermoFisher, Cat#NP0001) at 125 V for 110 min. Proteins were blotted onto a 0.45 μm nitrocellulose membrane (Merck, Amersham Protran, Cat#GE10600002) for 2 h at 4°C and 30 V. Membranes were washed with PBSTw (PBS supplemented with 0.1% Tween 20) twice followed by blocking for 1 h in PBS with 5% (w/v) soy protein isolate (Powerstar Food, Cat#psf-1131). Membranes were then incubated overnight at 4°C on a horizontal shaker with primary antibody in PBSTw supplemented with 0.5% (w/v) soy protein isolate. Membranes were then washed 4 times with PBSTw over 1 h and incubated with secondary antibody in PBSTw with 5% (w/v) soy protein isolate for 2 h on a horizontal shaker. Membranes were again washed 4 times with PBSTw over 1 h, rinsed with PBS twice and dried for 1 h. Images were acquired on an Amersham Typhoon imaging system (Cytiva).

Mouse anti-FLAG-M2 (Merck, Cat#F3165; dilution 1:5000) and Rabbit anti-Histone H3 (abcam Cat#ab1791; dilution 1:30,000) were used as primary antibodies. Goat anti-mouse-CF770 (Biotium, Cat#20077; dilution 1:10,000) and goat anti-rabbit-CF680 (Biotium, Cat#20067; dilution 1:10,000) were used as secondary antibodies.

Single-cell RNA-seq analysis of CRNeoblasts

Single-cell SmartSeq2 protocol was carried out as previously described (Li et al., 2021). Paired-end reads were mapped to the dd_Smed_v6 reference transcriptome (Rozanski et al., 2019) using Salmon (v1.4.0) (Patro et al., 2017). Downstream preprocessing and analysis were performed using estimated counts in the Salmon output, for which we summed up counts from different isoforms of the same gene. Cells with fewer than 2,400 genes detected were filtered out, passing 481 cells for downstream analysis. Raw gene counts were then normalized for sequencing coverage such that each cell had a total read count equal to that of the median library size for all cells. The resulting counts were added with a pseudo count of 1 and log-2 transformed. 2D embedding was performed with the SAM algorithm (version 0.8.1) (Tarashansky et al., 2019) using default parameters. $piwi-1^+$ cells were defined as those for which their log-2 transformed and normalized read counts were greater than zero. $piwi-1^+$ cells were clustered using the Leiden clustering algorithm, and each cluster was annotated using progenitor marker genes previously identified (N_epidermal: *soxP3*, dd_Smed_v6_5942_0_1; N_gut: *hnf*, dd_Smed_v6_1694_0_1; N_muscle: *pcdh11*, dd_Smed_v6_9283_0_1, cNeoblast: *tgs1*, dd_Smed_v6_10988_0_1) (Zeng et al., 2018).

QUANTIFICATION AND STATISTICAL ANALYSIS

All statistical tests were performed using Python 3.8 and the SciPy 1.8.0 stats package. Images were processed in ImageJ 1.53k, and single-cell segmentation and quantification was performed in scanR Analysis 3.2.0 (Olympus). Single-cell analysis was performed using Salmon (v1.4.0) for read mapping, and embedding was performed using the SAM algorithm (v0.8.1).